chemosensors

MDPI

Review

MOF-Derived Catalytic Interfaces for Low-Temperature Chemiresistive VOC Sensing in Complex Backgrounds

Lu Zhang [1], Shichao Zhao [1], Jiangwei Zhu [2] and Li Fu [1,*]

[1] College of Materials and Environmental Engineering, Hangzhou Dianzi University, Hangzhou 310018, China
[2] Co-Innovation Center for Sustainable Forestry in Southern China, Nanjing Forestry University, Nanjing 210037, China
* Correspondence: fuli@hdu.edu.cn

Abstract

The detection of volatile organic compounds (VOCs) at low operating temperatures is critical for public health, environmental monitoring, and industrial safety, yet it remains a significant challenge for conventional sensor technologies. Metal-organic frameworks (MOFs) have emerged as highly versatile precursors for creating advanced sensing materials. This review critically examines the transformation of MOFs into functional catalytic interfaces for low-temperature chemiresistive VOC sensing. We survey the key synthetic strategies, with a focus on controlled pyrolysis, that enable the conversion of insulating MOF precursors into semiconducting derivatives with tailored porosity, morphology, and catalytically active sites. This review establishes the crucial synthesis-structure-performance relationships that govern sensing behavior, analyzing how factors like calcination temperature and precursor composition dictate the final material's properties. We delve into the underlying chemiresistive sensing mechanisms, supported by evidence from advanced characterization techniques such as in situ DRIFTS and density functional theory (DFT) calculations, which elucidate the role of oxygen vacancies and heterojunctions in enhancing low-temperature catalytic activity. A central focus is placed on the persistent challenges of achieving high selectivity and robust performance in complex, real-world environments. We critically evaluate and compare strategies to mitigate interference from confounding gases and ambient humidity, including intrinsic material design and extrinsic system-level solutions like sensor arrays coupled with machine learning. Finally, this review synthesizes the current state of the art, identifies key bottlenecks related to stability and scalability, and provides a forward-looking perspective on emerging frontiers, including novel device architectures and computational co-design, to guide the future development of practical MOF-derived VOC sensors.

Keywords: metal-organic frameworks; MOF derivatives; chemiresistive sensors; volatile organic compounds; low-temperature sensing; catalysis; selectivity; anti-interference

check for updates

Received: 10 October 2025
Revised: 28 October 2025
Accepted: 31 October 2025
Published: 3 November 2025

Citation: Zhang, L.; Zhao, S.; Zhu, J.; Fu, L. MOF-Derived Catalytic Interfaces for Low-Temperature Chemiresistive VOC Sensing in Complex Backgrounds. *Chemosensors* **2025**, *13*, 386. https://doi.org/10.3390/chemosensors13110386

Copyright: © 2025 by the authors. Licensee MDPI, Basel, Switzerland. This article is an open access article distributed under the terms and conditions of the Creative Commons Attribution (CC BY) license (https://creativecommons.org/licenses/by/4.0/).

1. Introduction

Volatile organic compounds (VOCs) are a broad class of carbon-containing chemicals that readily vaporize at room temperature, leading to their ubiquitous presence in both indoor and outdoor environments [1]. Anthropogenic sources, including industrial processes, vehicle emissions, and off-gassing from paints, furniture, and consumer products, release a complex mixture of VOCs such as formaldehyde, benzene, toluene, and acetone into the atmosphere [2]. Prolonged exposure to these compounds poses significant risks to human

health, ranging from sick building syndrome and respiratory irritation to severe long-term effects, including carcinogenicity [3]. Furthermore, VOCs are key precursors in the formation of photochemical smog and ground-level ozone, contributing substantially to air pollution [4]. Beyond environmental monitoring, the analysis of specific VOCs in exhaled breath is emerging as a powerful, non-invasive tool for diagnosing and monitoring diseases, as these compounds can serve as biomarkers for metabolic or pathological conditions [5]. The critical need for real-time, on-site VOC monitoring has driven extensive research into gas sensor technologies. Among these, metal oxide semiconductor (MOS) sensors have been widely investigated and commercialized due to their high sensitivity, low cost, and simple design [6]. However, a fundamental limitation of traditional MOS sensors, such as those based on SnO_2 or ZnO, is their reliance on high operating temperatures, typically in the range of 200–500 °C [7]. This high thermal energy is required to overcome the activation energy barrier for the surface redox reactions between the target VOC and adsorbed oxygen species [8], which forms the basis of the sensing mechanism. This requirement leads to significant power consumption, limiting their application in portable, battery-operated devices, and introduces safety risks when detecting flammable or explosive VOCs [9]. Moreover, at these elevated temperatures, MOS sensors often exhibit poor selectivity, responding broadly to a wide range of reducing gases and making it difficult to distinguish a specific target analyte within a complex background mixture. These persistent challenges have created a strong impetus to develop new classes of sensing materials capable of efficient and selective VOC detection at or near room temperature (RT). While this remains a constraint for many MOS-only devices, it is important to note that RT operation has been realized in several polymer-involved and hybrid platforms. In particular, polymer/MOS hybrid films—such as chitosan–ZnO—have demonstrated RT detection of VOCs (e.g., acetone) with humidity-tolerant response, owing to proton-conduction pathways and acid–base interactions that modulate interfacial charge transport at RT [10]. Moreover, self-powered triboelectric-nanogenerator (TENG) architectures can harvest mechanical energy and transduce gas adsorption events without an external bias. For example, a respiration-driven TENG sensor employing a tin-oxide-doped polyethyleneimine (PEI/SnO_2) membrane functions dually as the triboelectric layer and the acetone-responsive interface, enabling RT breath-acetone monitoring under humid conditions. Broader reviews likewise document TENG-enabled chemical sensing of VOCs at RT with minimal power burden [11]. Together, these advances show that low-power/RT VOC sensing is feasible beyond heated MOS baselines; our review therefore positions MOF-derived catalytic interfaces as a complementary route that preserves RT/low-temperature operation while leveraging catalytic active sites and defect engineering to improve selectivity and robustness in complex backgrounds.

In the quest for next-generation sensing materials, metal-organic frameworks (MOFs) have attracted immense attention over the past two decades [12]. MOFs are a class of crystalline porous materials constructed from inorganic metal ions or clusters (nodes) linked together by polydentate organic ligands (linkers) [13]. This modular "building block" approach allows for an unprecedented degree of control over their structure and function, resulting in materials with exceptionally high specific surface areas (often exceeding 7000 cm^2/g), tunable pore sizes, and diverse chemical functionalities [14]. Initially, the application of MOFs in gas sensing focused on leveraging their extraordinary adsorption capabilities. The reversible and selective uptake of guest molecules within their pores can induce changes in mass, optical properties, or luminescence, which can be transduced into a sensing signal. However, a significant roadblock has hindered the direct application of pristine MOFs in chemiresistive sensors, particularly in the widely used chemiresistive sensor architecture. The vast majority of MOFs are electrical insulators or poor semiconductors, possessing low charge carrier mobility due to the insulating nature of the organic

linkers that separate the metal nodes [15]. This intrinsic lack of conductivity makes them unsuitable for devices that rely on measuring changes in electrical resistance. Furthermore, many common MOF structures exhibit limited stability in the presence of water vapor, a ubiquitous component of ambient air, which can lead to irreversible structural degradation and performance loss [16]. These fundamental limitations have catalyzed a crucial paradigm shift in the field. Instead of viewing MOFs as the final sensing material, researchers have increasingly begun to utilize them as highly engineered precursors or "sacrificial templates" to fabricate novel catalytic interfaces [17]. This approach involves the strategic thermal transformation (pyrolysis or calcination) of a carefully designed MOF precursor into a new material, typically a porous metal oxide, a nanostructured carbon, or a composite of the two. During this process, the organic linkers decompose, while the metal nodes are converted into highly dispersed, catalytically active metal or metal oxide nanoparticles. Crucially, the derivative material often inherits the high porosity, large surface area, and even the morphology of the parent MOF template. The resulting MOF-derived materials combine the desirable porous architecture of the precursor with the necessary semiconducting properties and catalytic activity of metal oxides or carbons, creating a functional interface perfectly suited for low-temperature chemiresistive VOC sensing. This conceptual evolution from MOFs as passive adsorbents to MOFs as pre-catalysts forms the central thesis of this review, providing a powerful and versatile platform to overcome the limitations of both traditional MOS materials and pristine MOFs [18].

This review provides a comprehensive and critical analysis of recent progress in the design, synthesis, and application of MOF-derived materials as catalytic interfaces for the low-temperature chemiresistive detection of VOCs. To clarify our contribution relative to existing reviews, we emphasize three differentiators. First, whereas recent comprehensive surveys cover pristine MOFs across multiple transduction modes and applications (chemiresistive, capacitive/impedimetric, FET, mass and optical) with a tutorial scope and broad MOF-based gas sensing [19], our focus is explicitly on MOF-derived catalytic interfaces (metal oxides/carbons and their heterostructures obtained by controlled pyrolysis/calcination) for chemiresistive VOC sensing. Second, rather than surveying all analytes, we target volatile organic compounds and the low-temperature ($\leq$~250 °C) regime, detailing how defect chemistry (oxygen vacancies), interfacial band engineering (p–n and n–n junctions), and hierarchical/hollow architectures inherited from MOFs jointly depress activation barriers for VOC oxidation and enlarge depletion-layer modulation. Such catalytic, temperature-focused analysis is outside the main scope of transducer-centric perspectives on pristine MOFs [20] and analyte-specific reviews on non-VOC targets such as H_2S [21]. Third, we treat complex backgrounds as a first-class design constraint—benchmarking strategies for humidity tolerance and interferent rejection (intrinsic catalytic bias, hydrophobic barriers) and system-level solutions (sensor arrays with machine-learning classification) relevant to portable operation. We integrate operando DRIFTS/XPS with DFT to connect these materials choices to observed selectivity and stability under realistic conditions. Framed this way, this review serves as a mechanistic and engineering playbook for translating MOF-derived interfaces into low-power, selective VOC chemiresistors that remain robust in humid, multi-gas environments.

The primary focus is on understanding the fundamental principles that enable these materials to operate efficiently and selectively, particularly in the context of complex environmental backgrounds. Here, we define a complex background as an atmosphere comprising (i) multiple organic interferents (e.g., ethanol, isopropanol, methanol, aldehydes, and aromatics such as toluene/xylene, often present at 10 ppb–100 ppm), (ii) inorganic oxidants/reductants ($NO_2/O_3/CO/H_2/CO_2$) at ambient-relevant levels, (iii) variable relative humidity (RH 10–95%), and (iv) slow or abrupt temperature fluctuations

(ΔT ≈ 5–15 °C). These factors perturb sensor signals via competitive adsorption, water-mediated surface chemistry and baseline drift, or redox side-reactions, and therefore must be considered in materials, device design, and benchmarking protocols. Section 2 details the key synthesis and engineering strategies used to transform MOF precursors into functional metal oxides, porous carbons, and heterostructured composites, establishing the critical synthesis-structure-performance relationships. Section 3 delves into the underlying chemiresistive sensing mechanisms, benchmarking the performance of state-of-the-art materials for key VOCs (e.g., acetone, formaldehyde) and highlighting insights gained from advanced mechanistic studies. Section 4 addresses the most significant challenges facing the practical application of these sensors—namely, selectivity, humidity interference, stability, and scalability—and critically evaluates the strategies being developed to overcome them. Finally, this review concludes with a summary of the field's current standing and a forward-looking perspective on emerging frontiers and future research directions.

2. Synthesis and Engineering of MOF-Derived Catalytic Interfaces

The transformation of MOFs into functional materials for chemiresistive sensing is a process of controlled deconstruction and reconstruction, where the initial, highly ordered framework is converted into a new architecture with the desired electronic and catalytic properties. The choice of the parent MOF and the specific transformation conditions are paramount, as they dictate the morphology, composition, porosity, and ultimately, the sensing performance of the final material.

2.1. Pyrolytic Transformation: From MOF to Functional Oxide/Carbon

The most prevalent and versatile method for preparing MOF-derived sensing materials is controlled thermal decomposition, commonly referred to as pyrolysis or calcination, in a controlled atmosphere. This process leverages the MOF as a hard template, where the metal nodes serve as a source for metal or metal oxide nanoparticles and the organic linkers act as a source for a carbon matrix [22]. During pyrolysis, the organic ligands decompose at elevated temperatures, leaving behind a porous structure composed of the metallic components [23], which are simultaneously converted into their corresponding oxides (in an oxidizing atmosphere like air) or metallic nanoparticles embedded within a carbon matrix (in an inert atmosphere like N_2 or Ar) [24].

The parameters of this thermal treatment—most notably the calcination temperature—are of critical importance, as they exert precise control over the final product's crystallinity, specific surface area, and defect concentration [25]. A non-linear, "Goldilocks" relationship exists between temperature and performance. If the temperature is too low, the organic linkers may not be fully removed, resulting in a poorly crystalline material with residual insulating carbonaceous species that block active sites and impede charge transport [26]. Conversely, if the temperature is too high, the delicate porous architecture inherited from the MOF precursor can collapse due to sintering and agglomeration of the nanoparticles [27]. This leads to a dramatic reduction in specific surface area and a loss of accessible active sites, which is detrimental to sensing performance. Consequently, an optimal calcination temperature must be identified for each MOF system to balance the complete removal of organic components with the preservation of a high-surface-area, porous nanostructure. For instance, in the synthesis of Co_3O_4 catalysts from ZIF-67 for toluene oxidation, a calcination temperature of 400 °C was found to be optimal, yielding high catalytic activity, whereas higher temperatures led to diminished performance [26]. Similarly, a study on MOF-5-derived ZnO nanoparticles for detecting microbial VOCs found that a calcination temperature of 600 °C yielded superior selectivity compared to materials prepared at either 450 °C or 800 °C, underscoring the necessity of systematic temperature optimization [28].

This templating strategy has been successfully applied to a wide range of MOF precursors to generate various catalytically active metal oxides. Zeolitic imidazolate frameworks (ZIFs), with their robust structures and nitrogen-rich linkers, are particularly popular precursors. For example, ZIF-8 (composed of Zn^{2+} nodes and 2-methylimidazole linkers) is widely used to synthesize porous ZnO with diverse morphologies [29], including nanocages and hierarchical structures, for sensing acetone and other VOCs [30]. Its cobalt analogue, ZIF-67, is a common precursor for producing p-type Co_3O_4 nanostructures for formaldehyde and acetone sensing [31]. Other MOF families, such as the UiO series (e.g., UiO-66 for ZrO_2 or TiO_2) and the MIL series (e.g., MIL-101 for Fe_2O_3) [32], have also been extensively used as templates to create a broad library of MOF-derived metal oxides with tailored properties [33]. Furthermore, when pyrolysis is conducted under an inert atmosphere, the nitrogen-containing linkers in precursors like ZIFs can be converted into N-doped porous carbon matrices [34]. These materials possess high electrical conductivity and a large number of active sites, making them excellent candidates for chemiresistive sensing platforms [35]. A schematic representation of the preparation of a ZnO@ZIF-8 nanorods array is shown in Figure 1. ZnO nanorods regarded as a sacrificial template, Zn^{2+} is etched by the ligand solution to induce ZIF-8 to growth on its surface, and ZnO@ZIF-8 nanorods with core–shell structure were successfully prepared.

Beyond composition, the MOF-to-oxide/carbon transformation frequently preserves key structural elements of the parent lattice. For ZIF-type precursors, controlled calcination yields hollow or hierarchical polyhedral ZnO/Co_3O_4 that retain the crystal-derived morphology and meso–micro-porosity, thereby shortening diffusion pathways and increasing the density of accessible catalytic/sensing sites [36]. Representative ZIF-8-derived hollow ZnO nanocages exhibit templated shape/porosity and strong gas-sensing responses, underscoring the role of inherited architecture in chemiresistive performance.

In parallel, the redox-active site landscape evolves with the thermal history and atmosphere. In oxidizing calcination, MOF-templated oxides often develop elevated oxygen-vacancy concentrations that stabilize reactive adsorbed oxygen at low temperature—both effects amplifying depletion-layer modulation under VOC exposure and thus the resistance change. Recent studies directly correlate vacancy (and O_{ads}) abundance with larger responses in chemiresistive ZnO/SnO_2 systems [37]. Because O 1s XPS assignments are frequently over-simplified, we note best practices for distinguishing lattice O, surface hydroxyls, and physisorbed/chemisorbed oxygen to substantiate vacancy claims [38]. Under inert pyrolysis, ZIF-derived carbons conserve nitrogen functionalities (graphitic/pyrrolic N) and can stabilize M–Nx motifs from metal nodes, yielding conductive, catalytically active M–N–C interfaces that facilitate charge transfer and low-overpotential surface redox steps relevant to VOC oxidation/electron return kinetics [39]. Likewise, ZIF-67-derived Co_3O_4 hollow nanocages exemplify how MOF-inherited inner/outer surfaces and defect populations enhance responses to aromatic VOCs at comparatively low temperatures [40].

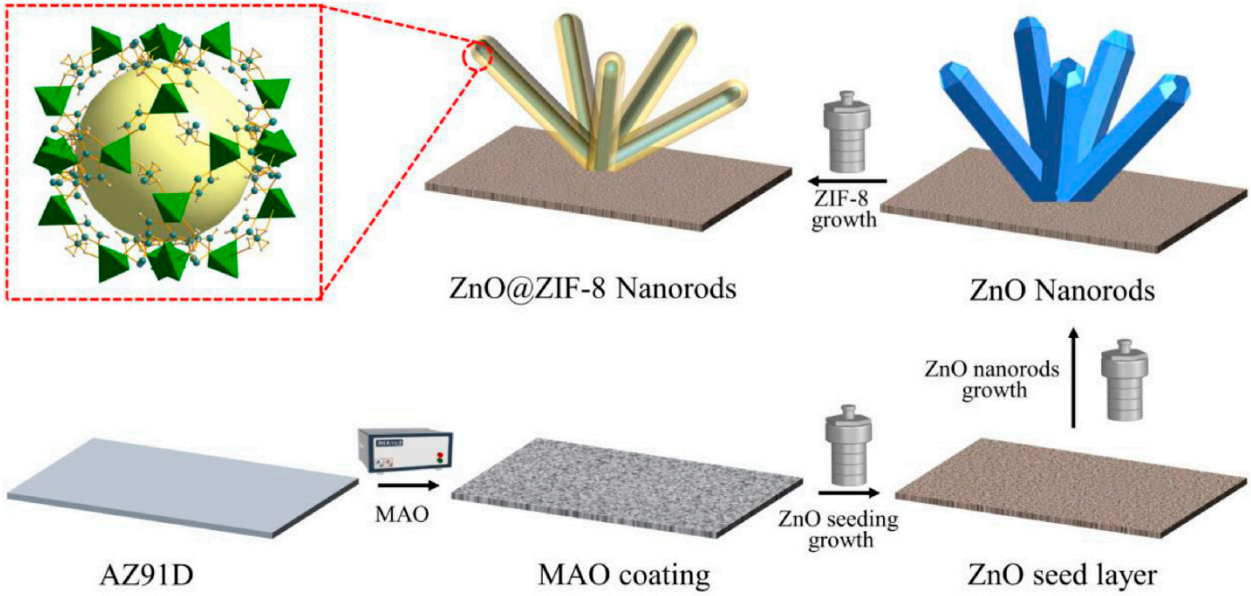


Figure 1. Schematic illustration of preparation of ZnO@ZIF-8 nanorods array (reproduced from [41], Under a Creative Commons license, Copyright 2023, KeAi).

2.2. Engineering Heterostructured and Bimetallic Interfaces

To further enhance the sensitivity and selectivity of MOF-derived sensors, researchers have moved beyond single-component materials to engineer more complex heterostructured and bimetallic interfaces. A particularly effective strategy involves the use of bimetallic or mixed-metal MOFs as precursors. In this approach, two or more different metal ions are incorporated into a single MOF crystal lattice during the initial synthesis. Subsequent pyrolysis of this atomically mixed precursor leads to the formation of composite materials, such as mixed metal oxides, alloys, or p-n/n-n heterojunctions, with an exceptionally high degree of interfacial contact [42].

This "single-pot" route to heterojunctions offers a distinct advantage over conventional methods that rely on the physical mixing of two separately synthesized nanomaterials. Because the constituent metals are intimately mixed at the atomic level within the parent MOF, the resulting oxide phases crystallize in extremely close proximity, ensuring a high density of well-defined interfaces in the final product [43]. These interfaces are crucial for enhancing sensing performance. For example, at the junction between a p-type (e.g., Co_3O_4) and an n-type (e.g., ZnO) semiconductor, a depletion region is formed due to charge carrier migration. This depletion region's width is highly sensitive to surface redox reactions with VOC molecules, leading to a much larger change in resistance compared to single-component materials and thus an amplified sensor response [44]. This effect has been demonstrated in various systems, such as Co_3O_4/Fe_2O_3 nanosheets derived from Co/Fe-MOFs for acetone sensing [45], SnO_2/NiO composites from Sn/Ni-MOFs for triethylamine detection, and $In_2O_3/BiVO_4$ composites from MOF precursors for n-butanol sensing [46]. The formation of a p-n heterojunction in a ZIF-8-derived Co_3O_4@ZnO microsphere is depicted in Figure 2. In addition to illustrating the interfacial depletion region, the figure also highlights two further aspects relevant to the sensing mechanism. First, the presence of Pt nanoparticles serves as a catalytic co-factor, accelerating surface redox reactions and facilitating rapid charge transfer across the heterojunction. Second, light irradiation promotes photoexcitation, generating additional charge carriers that modulate the depletion layer width and enhance the sensor's dynamic response. These synergistic effects collectively contribute to the improved sensitivity and selectivity observed in this system.

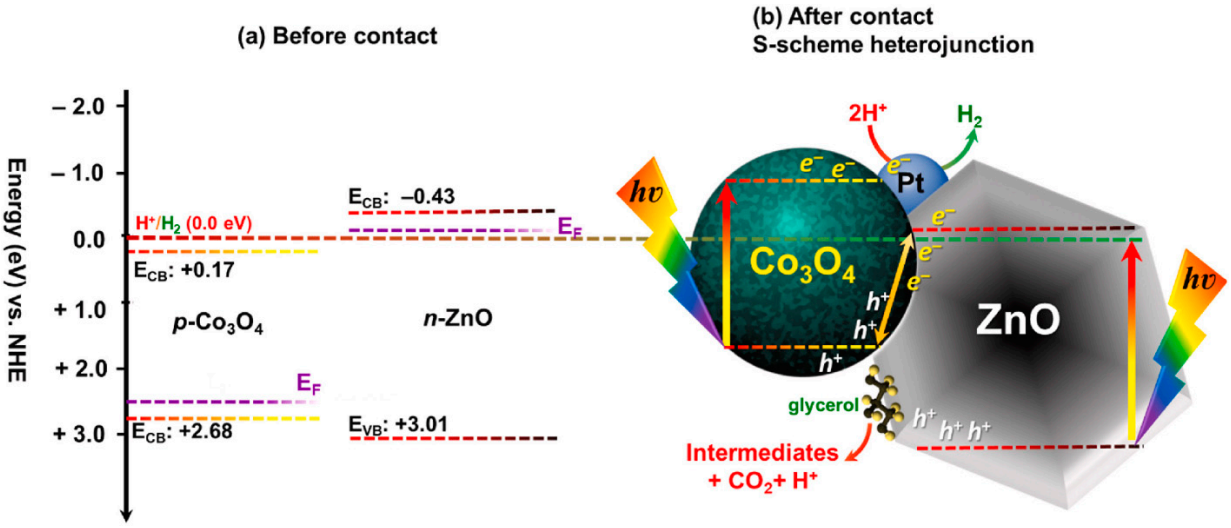


Figure 2. Schematic energy band diagram of the Co_3O_4@ZnO p-n heterojunction in air, illustrating the formation of a depletion layer at the interface that modulates the sensor's resistance (reproduced from [47]; Copyright 2022, Elsevier).

2.3. Templating Hierarchical and Hollow Architectures

One of the most compelling advantages of using MOFs as templates is the ability to preserve the precursor's morphology, leading to the formation of derivatives with unique hierarchical and hollow architectures [31,48]. For example, the pyrolysis of rhombic dodecahedral crystals of ZIF-8 or ZIF-67 often yields hollow nanocages or porous polyhedra of ZnO or Co_3O_4 that retain the shape of the parent crystal [36,49]. A representative SEM image of hierarchical Co_3O_4 derived from a Co-MOF is shown in Figure 3.

These complex architectures are not merely an aesthetic outcome of the synthesis; they play a crucial functional role in enhancing sensing performance, especially at low temperatures. The hierarchical structure, typically comprising interconnected macropores, mesopores, and micropores, provides an efficient network for gas transport. The larger pores act as highways, allowing VOC molecules to rapidly diffuse from the bulk atmosphere into the interior of the sensing material, while the smaller pores provide the high surface area necessary for adsorption and reaction6. This facilitated mass transport is critical for achieving fast response and recovery times, as gas diffusion can become a rate-limiting step at lower operating temperatures. Studies comparing hollow versus solid nanostructures have consistently shown that the hollow morphology leads to superior sensing performance, attributed to the increased number of accessible active sites on both the inner and outer surfaces and the reduced diffusion path length for gas molecules [36,50]. This morphological control, inherited directly from the well-defined crystalline structure of the MOF precursor, represents a key advantage of the MOF-derived approach over conventional synthesis methods for metal oxides.

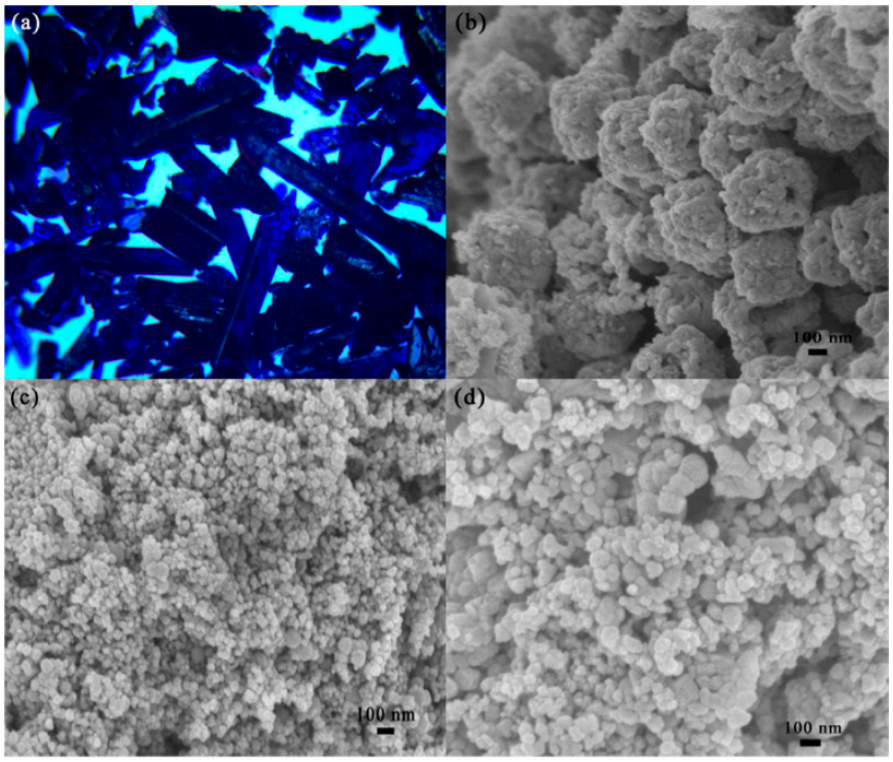


Figure 3. (**a**) Optical microscopy of Co-MOF; SEM images of the (**b**) Co_3O_4-350 sphere, (**c**) Co_3O_4-400 and (**d**) Co_3O_4-450, respectively (reproduced from [51]; Copyright 2017, American Chemical Society).

To summarize the relationship between the synthetic approach and the resulting material properties, Table 1 provides an overview of common MOF precursors and the structural features of their derivatives. ZIF-type precursors (e.g., ZIF-8, ZIF-67) reliably transform, via 350–600 °C calcination, into defect-rich ZnO or Co_3O_4 that preserve polyhedral/hollow morphologies and create short diffusion paths. In ZIF-67→Co_3O_4, a "Goldilocks" temperature (~400 °C) maximizes O_{ads}/O_{latt} and Co^{3+}/Co^{2+} ratios, yielding superior low-temperature aromatic VOC oxidation and, by extension, strong chemiresistive responses (toluene T90 ≈ 225–240 °C in catalysis) [26]. Fe-modified IRMOF-3 produces ZnO/$ZnFe_2O_4$ hollow cubes; the inherited hierarchical shells and n–n junctions increase surface-adsorbed oxygen and enlarge depletion-layer modulation, enabling high acetone response even at 200–250 °C [52]. Sn-MOF precursors yield porous, nanoparticle-piled SnO_2 with abundant adsorbed oxygen; formaldehyde sensing reaches ultrahigh response (~10,000 at 10 ppm) at 120 °C, highlighting vacancy-assisted low-T redox. UiO-family calcination affords thermally robust ZrO_2 (and ZrO_2@C), valuable as stable supports/barriers, while MIL-101(Fe) and PBAs generate Fe-/spinel-oxides that can be tuned into core–shell or triple-shelled hollow architectures for enhanced transport and interfacial band engineering. Bimetallic MOFs (e.g., Zn/Co ZIFs) give intimately mixed Co_3O_4@ZnO p–n junctions that amplify resistance swings at ≤250 °C by widening/narrowing depletion regions under VOC exposure. Finally, inert-atmosphere pyrolysis of N-rich MOFs furnishes conductive M–N–C scaffolds that stabilize active M–N_x sites and facilitate room-/low-temperature charge transfer, complementing oxide pathways in hybrid interfaces. Taken together, the precursor choice dictates the accessible defect chemistry (vacancies, O_{ads}), heterointerfaces (p–n, n–n), and hierarchical porosity; the thermal program sets their balance. These coupled factors—not surface area alone—explain why ZIF-derived oxides, IRMOF-derived heterojunctions, and Sn-MOF-derived SnO_2 repeatedly deliver the best ≤250 °C VOC performance.

Table 1. Synthesis strategies for MOF-derived materials and their influence on physicochemical properties.

MOF Precursor	Synthesis Method	Key Parameters	Derived Material	Key Structural Features	References
ZIF-8	Pyrolysis in air	400–600 °C	Porous ZnO	Hollow nanocages, polyhedra, high surface area	[30]
ZIF-67	Pyrolysis in air	350–500 °C	Porous Co_3O_4	Hierarchical porous structure, hollow nanocubes	[31]
Bimetallic ZIF (Zn/Co)	Pyrolysis in air	500 °C	Co_3O_4@ZnO	p-n heterojunction, porous microspheres	[45]
UiO-66	Calcination	500–600 °C	Porous ZrO_2	Retained crystal morphology, high thermal stability	[53]
MIL-101(Fe)	Pyrolysis	>330 °C	Fe_2O_3/Carbon	Porous iron oxide with carbon matrix	[54]
Bimetallic PBA (M/Fe)	Calcination	400–600 °C	MFe_2O_4 Spinel Oxides	Inverse/normal spinel structures, nanocubes	[55]
MOF-5 (Zn)	Calcination	450–800 °C	ZnO nanoparticles	Controllable crystallite size	[56]
ZIF-8	Calcination/ Pyrolysis	300–600 °C	N-doped ZnO	Porous/hollow ZnO with N-defects, increased surface O^-	[57]
ZIF-8	Calcination + Ag loading	450–600 °C	ZnO/Ag micro-octahedra	Plasmonic sites, abundant grain boundaries	[58]
ZIF-8	Pyrolysis; Ag nanocrystal decoration	450–600 °C	Ag–ZnO hollow structures	Hollow cages, highly dispersed Ag, boosted TEA sensing	[59]
ZIF-67	Pyrolysis	350–500 °C	Co_3O_4 hollow nanocages	Double-shelled/hollow dodecahedra, rich lattice O	[60]
ZIF-67 → ZIF-67@ZIF-8 (core–shell)	MOF@MOF then calcination	400–600 °C	Co_3O_4/ZnO nano-heterostructure	Core–shell-derived p–n junction, mesoporous	[61]
ZIF-8 (with Cu modification)	Ion-exchange + calcination	450–600 °C	CuO/ZnO hollow nanocages	Hollow polyhedra, multiple redox sites	[62]
UiO-66	Calcination	500–700 °C	ZrO_2@C	Mesoporous ZrO_2 with carbon residue; temperature-tunable pores	[63]
UiO-66	Derived coating via calcination	—	ZrO_2 protective layer	Conformal, porous ZrO_2 film; high thermal stability	[64]

Table 1. *Cont.*

MOF Precursor	Synthesis Method	Key Parameters	Derived Material	Key Structural Features	References
MIL-101(Fe)	Pyrolysis	700–800 °C	Fe_2O_3/C composite	Porous Fe_2O_3 embedded in conductive carbon	[65]
Prussian Blue Analogue (Co/Fe)	Annealing	350–500 °C	$CoFe_2O_4$ nanocubes	Spinel nanocubes from PBA template	[66]
MOF-5 (Zn)	Calcination of Pd@MOF-5	400–600 °C	Pd/PdO@ZnO	Noble-metal-sensitized ZnO, abundant oxygen vacancies	[67]
UiO-66 (Zr) + Cu source	Calcination	—	Cu NWs@ZrO_2	Metal/ZrO_2 composite with uniform MOF-derived ZrO_2	[68]

3. Electrochemical Sensing Mechanisms and Performance Analysis

The superior performance of MOF-derived materials in low-temperature VOC sensing stems from their unique combination of semiconducting properties, high surface area, and exceptional catalytic activity. Understanding the fundamental mechanisms by which these materials interact with VOC molecules is essential for rational design and further optimization. For chemiresistive sensors, the response is defined as a ratio between the electrical resistance in dry air (R_a) and in the target gas (R_g). For reducing gases such as acetone and formaldehyde, the response is calculated as R_a divided by R_g. For oxidizing gases such as NO_2 and O_3, the response is calculated as R_g divided by R_a. When the response is reported as a normalized percentage change, it is expressed as S%. For reducing gases, S% is calculated as ($R_a - R_g$) divided by Ra and multiplied by 100. For oxidizing gases, S% is calculated as ($R_g - R_a$) divided by R_g and multiplied by 100. Sensitivity is distinct from response and refers specifically to the slope of the calibration curve over a defined concentration range. For chemiresistive sensors, sensitivity is calculated as the change in response divided by the change in analyte concentration, with units of ppm^{-1} or ppb^{-1}. When the signal is expressed as S%, sensitivity corresponds to the change in S% per unit change in analyte concentration, with units of $\%{\cdot}ppm^{-1}$. For amperometric or voltammetric sensors, sensitivity is determined in the same way, based on the slope of the current versus analyte concentration plot. The typical units are amperes per ppm ($A{\cdot}ppm^{-1}$) or microamperes per ppm ($\mu A{\cdot}ppm^{-1}$), and measurements are made under specified potential and electrolyte conditions.

3.1. Low-Temperature Catalytic Sensing Mechanisms

The operating principle of chemiresistive sensors based on MOF-derived semiconductors is rooted in the modulation of charge carrier concentration at the material's surface [69]. For an n-type semiconductor like ZnO or SnO_2, in ambient air, atmospheric oxygen molecules adsorb onto the surface and capture free electrons from the conduction band to form ionized oxygen species (such as O_2^-, O^-), with the dominant species depending on the operating temperature [7]. This process creates an electron-depleted layer near the surface, significantly increasing the material's electrical resistance [70]. When the sensor is exposed to a reducing VOC (e.g., acetone, formaldehyde), the VOC molecules are catalytically oxidized by these surface oxygen species [71]. This reaction releases the

trapped electrons back into the conduction band, which narrows the depletion layer and causes a measurable decrease in resistance [72]. For a p-type semiconductor like Co_3O_4 or NiO, the process is analogous but involves holes as the majority charge carriers, leading to an increase in resistance upon exposure to a reducing VOC.

What distinguishes MOF-derived materials is their ability to facilitate this redox cycle at much lower temperatures than conventional MOS materials [73]. This enhanced low-temperature activity is not merely a consequence of their high surface area, but is intrinsically linked to their catalytic nature. The pyrolysis of MOF precursors often generates a high density of structural defects, particularly oxygen vacancies, on the surface of the resulting metal oxide nanoparticles [17,74]. These oxygen vacancies serve as dual-function active sites. Firstly, they are highly favorable locations for the adsorption and activation of atmospheric oxygen, increasing the concentration of reactive oxygen species available on the surface. Secondly, these coordinatively unsaturated metal sites can also directly interact with and activate the C-H or O-H bonds within the VOC molecule, lowering the activation energy barrier for its oxidation [75]. Therefore, a high concentration of oxygen vacancies directly correlates to both a greater abundance of reactants (adsorbed oxygen) and a higher intrinsic catalytic turnover rate. This "defect engineering," naturally achieved through the MOF templating method, is a cornerstone of the low-temperature sensing capability of these materials [76].

Quantitatively, MOF-templated oxides already exhibit low-temperature VOC sensing consistent with this defect-catalysis picture. For instance, $ZnO/ZnFe_2O_4$ hierarchical hollow cubes (Figure 4) obtained by calcining an Fe^{3+}-modified IRMOF-3 precursor show high acetone responses at comparatively low working temperatures: an optimal 200–250 °C window, with a response of ~2.4 even at 0.5 ppm and 9.4 at 5 ppm (R_{air}/R_{gas}) at 250 °C. Importantly, O 1s XPS deconvolution reveals a larger fraction of surface-adsorbed oxygen for the MOF-derived heterostructure (29.4%) than for singular ZnO (23.7%), linking vacancy-associated O_{ads} abundance to the observed signal gain; response/recovery times remain in the several-minute range across 0.5–5 ppm, reflecting adsorption–desorption kinetics at low dose [52]. Likewise, a p-type exemplar—3D hierarchical Co_3O_4 derived from Co-cluster MOF microcrystals—detects formaldehyde at 170 °C with a reported detection limit of 10 ppm and 30-day stability, validating that MOF-derived microstructures and defect populations can sustain low-temperature redox cycling while preserving baseline integrity over time [51].

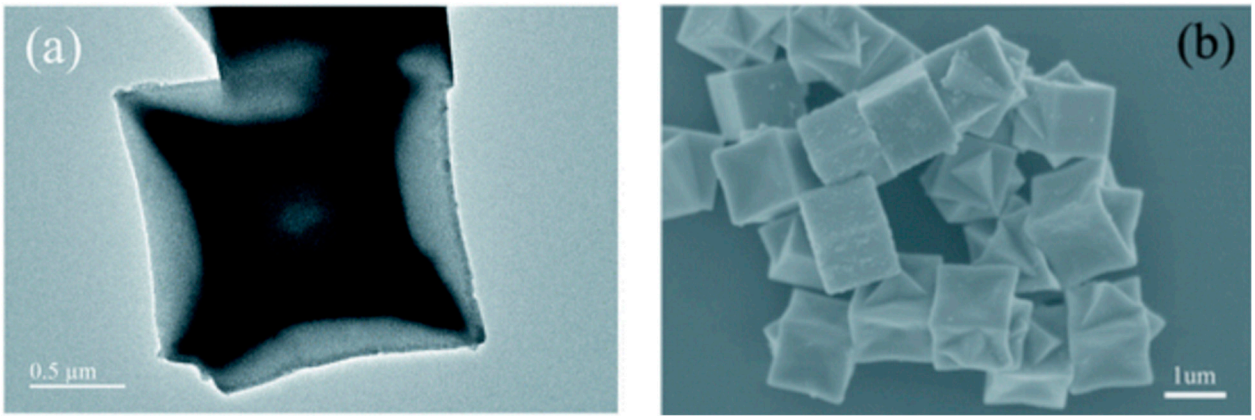


Figure 4. (**a**) TEM and (**b**) SEM image of $ZnO/ZnFe_2O_4$ hierarchical hollow cubes (reproduced from [52] Under a Creative Commons license, Copyright 2017, RSC).

In this regime, MOF-templated calcination or pyrolysis creates defect-rich oxides and intimate heterojunctions that lower activation barriers for O formation and VOC oxidation

while preserving short diffusion paths from hollow/Hier architectures. Representative exemplars include IRMOF-3-derived $ZnO/ZnFe_2O_4$ hollow cubes that detect acetone in the 200–250 °C window ($R_{air}/R_{gas} \approx 9.4$ at 5 ppm, attributed to high O_{ads} and n–n junctions) [52]. Sn-MOF-derived laminar SnO_2 reaches ultrahigh formaldehyde response (≈10,000 at 10 ppm) at 120 °C with 33/142 s response/recovery, linked to rich adsorbed oxygen and nanoparticle-piled porosity [77]. For aromatics/acetone, ZIF-derived Co_3O_4 shows strong signals at 140–225 °C, with low ppm LOD and p-type band-edge modulation amplified by vacancy engineering and (when present) noble-metal or oxide junctions [31]. Practically, ≤250 °C operation reduces power and improves safety for flammable VOCs; we therefore benchmark responses (R_a/R_g), sensitivity (ppm^{-1} or $\%{\cdot}ppm^{-1}$), LOD, T_{opt}, and humidity tolerance as the most relevant figures of merit in this temperature band.

Critically, these data nuance the qualitative mechanism above. In the n-type $ZnO/ZnFe_2O_4$ case, both heterojunction band alignment and a measurable increase in O_{ads} (a proxy for oxygen-vacancy–mediated sites) contribute to larger depletion-layer modulation upon VOC oxidation; the improvement is therefore not only "more surface area," but a demonstrable shift in surface chemistry that raises the steady-state density of reactive oxygen and accelerates electron return to the conduction band [52]. In contrast, the p-type Co_3O_4 example shows that hierarchical, MOF-inherited porosity and defect chemistry can lower the temperature for formaldehyde oxidation while maintaining long-term stability of hole transport, with the expected resistance increase under reducing VOCs [51]. Together, these cases support the view that "defect engineering" is most effective when coupled to interfacial design (e.g., n–n or p–n contacts) that tunes band bending and charge-carrier lifetimes. They also caution against a simplistic "more vacancies is always better" heuristic: vacancy-rich surfaces raise O_{ads} and catalytic turnover, but can slow desorption or introduce baseline drift if not balanced by morphology (mass transport) and interface design. Future reports should therefore pair vacancy metrics (e.g., O_ads/O_latt by XPS, EPR) with activation parameters and humidity-dependent response to disambiguate catalytic from transport limitations at ≤200–250 °C.

3.2. Performance Benchmarking for Key VOCs

The efficacy of the MOF-derived approach is best illustrated by examining the performance of sensors developed for specific, high-impact VOCs.

3.2.1. Acetone Sensing

Acetone is a crucial biomarker for diabetes mellitus (detectable in exhaled breath) and a widely used industrial solvent, making its sensitive detection a significant goal. MOF-derived materials have demonstrated exceptional performance in this area. For instance, hierarchical ZnO micro-dodecahedra/flower structures, synthesized by modifying a ZIF-8 precursor with sulfuric acid before calcination [30], exhibited a remarkable response of ~120.6 to 100 ppm acetone at 350 °C, which was 30 times higher than the pristine ZIF-8-derived ZnO [78]. The enhancement was attributed to an increased specific surface area and more efficient gas transport channels created by the acid treatment. Similarly, hierarchical porous Co_3O_4 derived from a Co-MOF template showed a high response of 27.6 to 50 ppm acetone at a significantly lower operating temperature of 140 °C, with a low detection limit of 0.1 ppm [79]. The development of bimetallic spinel oxides, such as $NiFe_2O_4$ nanocubes derived from MOF templates, has also proven effective, demonstrating high selectivity towards acetone with a detection limit as low as 1 ppm [55]. These examples highlight how morphological control and compositional engineering via MOF templates can yield high-performance acetone sensors. A summary of representative MOF-derived acetone sensors is provided in Table 2.

Table 2. Comparative performance of MOF-derived sensors for acetone detection.

Sensing Material	Operating Temp. (°C)	Target Conc. (ppm)	Response (Ra/Rg or S%)	Response/Recovery Time (s)	LOD (ppb/ppm)	References
MOF-derived Co_3O_4	140	50	27.6	-/-	0.1 ppm	[31]
ZIF-8 derived Co_3O_4@ZnO	280	50	~18	15/19	0.5 ppm	[45]
MOF-derived $NiFe_2O_4$	240	100	~15	13/8	1 ppm	[55]
Bi-gallate MOF/CS/IL	60	10	~1.5	15/3	<10 ppm	[80]

3.2.2. Formaldehyde Sensing

Formaldehyde (HCHO) is a primary indoor air pollutant and a known human carcinogen, demanding sensors with ultra-high sensitivity for early warning and exposure monitoring [77]. MOF-derived materials have achieved breakthrough performance in HCHO detection. In a remarkable demonstration, laminar SnO_2 derived from a Sn-MOF precursor exhibited an ultrahigh response value of 10,000 towards just 10 ppm of HCHO at a low operating temperature of 120 °C [77]. This extraordinary sensitivity was attributed to the material's rich adsorbed oxygen content and unique nanoparticle-piled porous structure. Another effective strategy involves deriving hierarchical Co_3O_4 nanostructures from Co-cluster-based MOFs, which enabled efficient HCHO detection at 170 °C with a low detection limit of 10 ppm and excellent long-term stability over 30 days [51]. Composites have also shown great promise; for example, Zn^{2+}-doped SnO_2 hollow nanofibers derived from MOF templates via electrospinning demonstrated a high response of 25.7 towards 100 ppm HCHO [81], showcasing the synergy between hollow nanostructures and catalytic doping [82]. These results underscore the potential of MOF-derived materials to meet the stringent requirements for trace-level HCHO sensing. Table 3 compares the performance of several notable MOF-derived formaldehyde sensors.

Table 3. Comparative performance of MOF-derived sensors for formaldehyde detection.

Sensing Material	Operating Temp. (°C)	Target Conc. (ppm)	Response (Ra/Rg or S%)	Response/Recovery Time (s)	LOD (ppb/ppm)	References
Sn-MOF derived SnO_2	120	10	10,000	33/142	<10 ppb	[77]
Co5-MOF derived Co_3O_4	170	200	~14	-/-	10 ppm	[51]
ZIF-67 derived Cu-Co Oxides	108	50	90% conversion	-/-	-	[83]
MOF-derived ZZS HNFs	220	100	25.7	12/18	-	[82]
MOF-derived porous SnO_2 prisms	120	2	882	19/–	–	[84]
MOF-derived ZnO (UV-assisted)	~25 (UV on)	–	–	–	100 ppb	[85]
Pt/ZnO–In_2O_3 hollow nanofibers (derived from Pt@ZIF-8)	180	100	48.3	5/22	74.6 ppb	[86]
Co-MOF-derived Co_3O_4 (3D)	170	100	–	–	10 ppm	[51]
ZIF-67-assisted Co_3O_4/In_2O_3 composite (MOF-templated)	–	10	(improved vs. In_2O_3)	–	–	[34]

3.2.3. Benzene and Aromatic VOCs Sensing

The detection of aromatic VOCs like benzene, toluene, and xylene (BTX) is crucial due to their toxicity and widespread industrial use. MOF-derived materials are being explored for this purpose, with strategies often focusing on enhancing surface interactions with the aromatic rings of the analytes [20]. For example, materials derived from the MIL-101 MOF, which contains benzenedicarboxylate linkers, are promising candidates for creating Fe_2O_3 or Cr_2O_3 catalysts with an affinity for aromatic compounds [87]. The carbon matrices derived from such MOFs can also engage in π-π stacking interactions with benzene, enhancing adsorption and selectivity [88]. While research in this specific area is less mature than for acetone or formaldehyde, the inherent tunability of MOF precursors provides a clear pathway for designing materials with tailored surface chemistry for the selective detection of aromatic VOCs. Quantitatively, ZIF-67-derived hollow hierarchical Co_3O_4 nanocages already deliver very strong responses to methylbenzenes—e.g., Ra/Rg = 78.6 to 5 ppm p-xylene and 43.8 to 5 ppm toluene at 225 °C—attributed to their thin-shelled, mesoporous architecture and high catalytic activity [40]. For benzene specifically, MOF-derived Co_3O_4/TiO_2 heterostructures with 1.0 wt% Fe show low-ppm operability, detecting 0.35–2.0 ppm benzene with an optimal temperature of ~175 °C, underscoring how heterojunctions and controlled oxygen activation help compensate for benzene's weaker adsorption compared with methylbenzenes [89]. The gas sensing mechanism of Co_3O_4 nanoparticles decorated with Ag. In ambient air (Figure 5a,c), oxygen molecules are chemisorbed on the surface of Co_3O_4 and capture electrons from the valence band to form O^- species, resulting in the formation of a hole accumulation layer. This increases the sensor's baseline resistance. In humid air, H_2O molecules (blue spheres) may also be weakly adsorbed but have minimal effect on the charge depletion/accumulation layer. When exposed to $C_6H_5CH_3$ (toluene) molecules (green spheres), these reducing gas molecules react with the adsorbed O^- species, releasing trapped electrons back into the semiconductor and thinning the hole accumulation layer (Figure 5b,d). Consequently, the resistance of the p-type semiconductor decreases, which constitutes the sensor signal. The presence of Ag nanoparticles (yellow spheres) accelerates the surface reaction through spillover effects, enhancing both the adsorption kinetics and electron transfer efficiency. This results in faster response and recovery times. Pushing temperatures lower, Ag-modified Co_3O_4 obtained from ZIF-67 achieves a response of ~520.6 to 100 ppm toluene at 150 °C—about a 21× jump over undoped Co_3O_4—indicating that noble-metal spillover and d-band tuning can meaningfully depress the activation barrier for aromatic oxidation while preserving high signal gain (Figure 5) [90]. Together these data reveal a nuanced picture. First, xylene/toluene typically respond more strongly than benzene at comparable loadings and morphologies, consistent with higher polarizability and stronger π-interactions; however, Fe-loaded Co_3O_4/TiO_2 shows that judicious lattice-oxygen management and p–n junctions can narrow this gap at lower temperatures by accelerating surface redox rather than relying solely on adsorption strength [40,89]. Second, MOF-derived carbons are often credited with π-π stacking, yet the largest response gains in BTX sensing come when that adsorption bias is coupled to catalytic pathways (e.g., Ag-assisted O_2 activation) that convert adsorption events into electron-transfer efficiently at $\leq$150–200 °C [40,90]. Third, most BTX exemplars remain chemiresistive and operate above ambient; translation to strictly electrochemical transduction in humid, multi-analyte backgrounds will require (i) co-designed catalytic sites that selectively activate the aromatic ring without over-oxidation, (ii) conductive MOF-derived scaffolds that maintain percolation at low bias, and (iii) rigorous cross-interference tests (ethanol/acetone/NO_x) at realistic RH. In short, the BTX literature validates the promise of MOF-derived interfaces, but it also shows that selective benzene sensing at low

temperature depends less on π-stacking alone and more on engineered interfacial redox and heterojunction energetics that convert weak adsorption into large, selective signals.

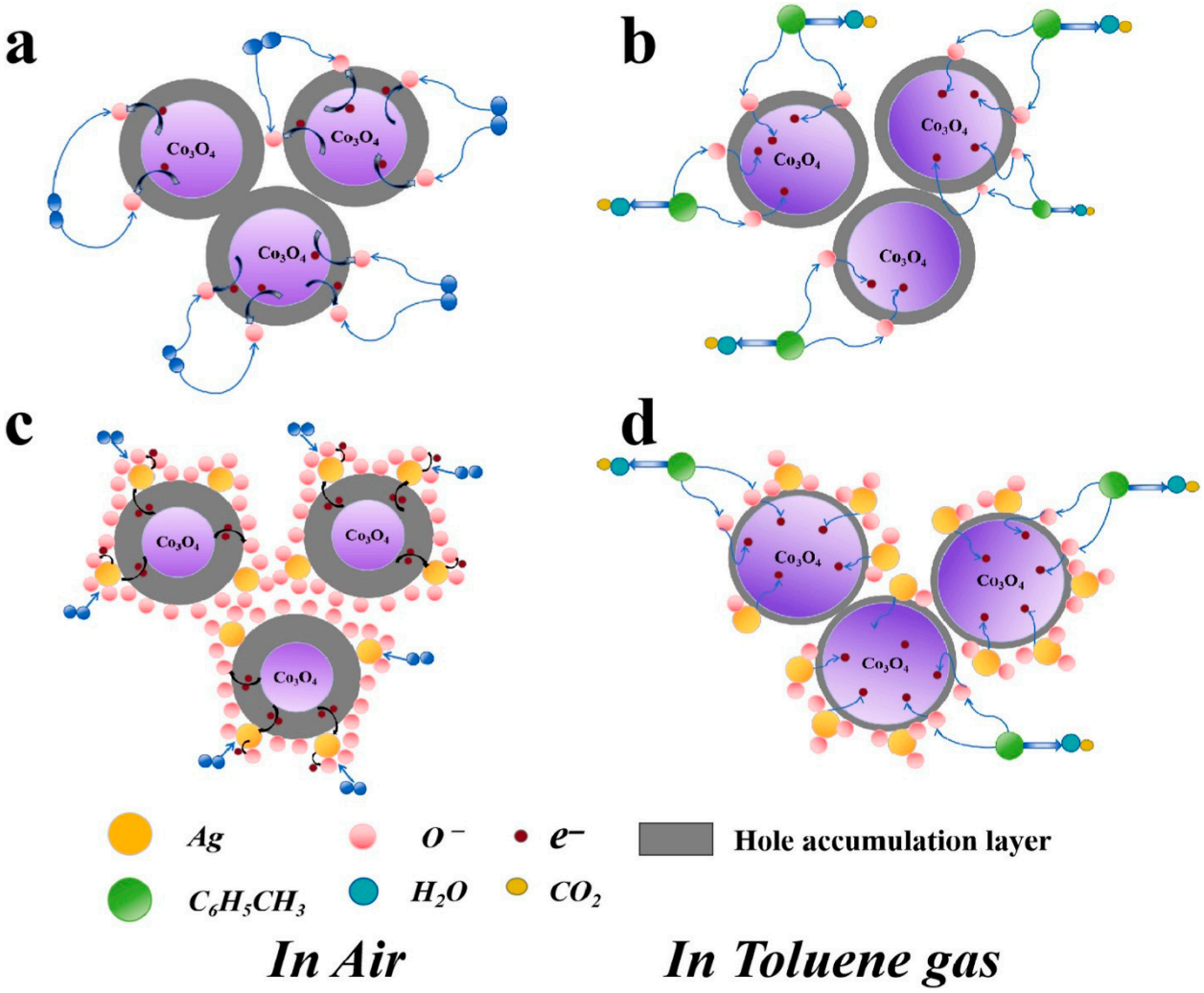


Figure 5. Schematic illustration of the gas sensing mechanism of Ag-decorated Co_3O_4 nanoparticles. (**a**,**c**) represent the sensor surface in ambient air: oxygen molecules are chemisorbed and capture electrons from the Co_3O_4 valence band to form O^- species, creating a hole accumulation layer (gray shell). (**b**,**d**) represent the sensor in the presence of toluene gas: reducing gas molecules react with the adsorbed oxygen species, releasing electrons and thinning the hole accumulation layer, leading to decreased resistance. Legend: Yellow spheres = Ag nanoparticles; green spheres = toluene molecules ($C_6H_5CH_3$); pink spheres = adsorbed O^- species; blue spheres = water molecules; small brown dots = electrons (e^-); gray shell = hole accumulation layer. Arrows indicate the direction of electron transfer and surface reaction (reproduced from [90]; Copyright 2025, Elsevier).

3.2.4. Ethanol Sensing

Ethanol is a dominant indoor interferent and a regulated flammable VOC; benchmarking MOF-derived interfaces for ethanol helps assess selectivity against alcohols in complex backgrounds. Representative MOF-templated oxides already demonstrate strong low-temperature performance. Au-decorated mesoporous ZnO derived from ZIF-8 (Au/ZnO–ZIF-8) achieves a response factor of ~37.7 to 100 ppm ethanol at 250 °C with ~19/9 s response/recovery; DFT attributes the gain to Au–ZnO Schottky junctions and enhanced adsorption energy (−1.81 eV vs. −0.22 eV for pristine ZnO) [91]. ZIF-assisted p–n heterojunctions also lower the operating temperature: TiO_2/Co_3O_4 "necklace-like" fibers assembled with MOF-derived Co_3O_4 report ~16.7 (150 ppm) at 150 °C [92]. Recent

MOF-derived mixed oxides further push selectivity and LOD: ZnO/Co_3O_4 composites obtained via MOF templating deliver higher ethanol sensitivity at reduced Topt with sub-ppm LOD (~0.5 ppm), attributed to porous architectures and abundant heterointerfaces that amplify depletion-layer modulation. Noble-metal spillover on MOF-derived Co_3O_4 hollow polyhedra (typically from ZIF-67) enhances kinetics at $\leq$150 °C and accelerates response (e.g., Pd/Co_3O_4 HP: ~12 s response at 150 °C), highlighting a catalytic route to low-T operation [49]. Benchmarking note: for ethanol we report R_a/R_g (or S%), LOD, Topt, and humidity robustness to align with Sections 3.2.1 and 3.2.2 and enable cross-VOC comparisons.

3.3. Advanced Mechanistic Investigations

To move beyond empirical optimization and enable rational design, it is crucial to probe the fundamental reaction mechanisms at the catalyst-gas interface. Advanced in-situ and computational techniques are providing unprecedented insights into these processes.

In-situ Diffuse Reflectance Infrared Fourier Transform Spectroscopy (DRIFTS) is a powerful tool that allows researchers to monitor the vibrational signatures of molecules adsorbed on the catalyst surface under realistic reaction conditions [93]. By tracking the appearance and disappearance of specific infrared bands over time or as a function of temperature, one can identify key reaction intermediates and map out the catalytic cycle [94]. For example, in-situ DRIFTS studies on the oxidation of toluene over a MOF-derived Co-Fe-δ-MnO_2 catalyst revealed the formation of benzoate species as key intermediates, confirming that the reaction proceeds via the Mars-van Krevelen mechanism [95], where lattice oxygen from the catalyst participates in the oxidation [96]. Similarly, a study on formaldehyde oxidation over ZIF-67-derived Cu-Co mixed oxides identified dioxymethylene, formate, and carbonate species as the primary intermediates [97], elucidating the stepwise pathway from HCHO to CO_2 [83]. These studies provide direct spectroscopic evidence of the catalytic processes occurring on the sensor surface. Figure 6 displays typical DRIFTS spectra showing the evolution of surface intermediates during a catalytic reaction.

Complementing these experimental techniques, computational methods, particularly Density Functional Theory (DFT), offer an atomic-level understanding of the interactions between VOCs and the sensor surface [98]. DFT calculations can determine the most stable adsorption geometries for different VOC molecules on specific crystal facets of the MOF-derived material, calculate their binding energies [99], and map the potential energy surface for their dissociation and oxidation [80]. This allows researchers to identify the most active catalytic sites (e.g., defect sites, metal adatoms) [100] and understand the origin of selectivity [101]. For instance, DFT can explain why a particular surface has a higher adsorption energy for acetone than for ethanol, providing a theoretical basis for its observed selectivity [102,103]. By combining the macroscopic performance data, the real-time observations from in-situ spectroscopy, and the atomic-scale insights from DFT, a holistic and predictive understanding of the sensing mechanism can be constructed.

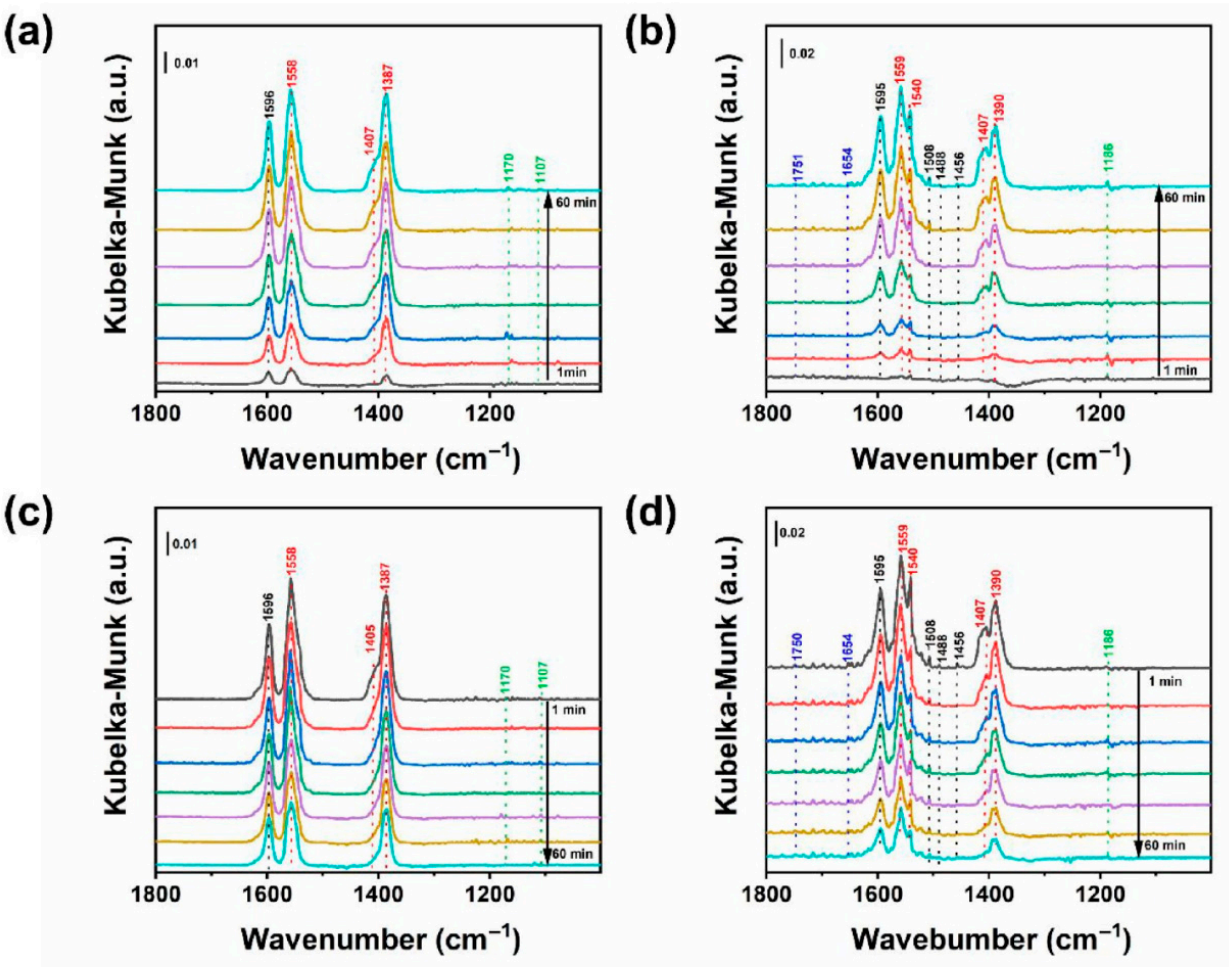


Figure 6. DRIFTS spectra of toluene adsorption (**a**,**b**) and oxidation (**c**,**d**) on δ-MnO_2 and Co−Fe-δ-MnO_2-20% at 230 °C, respectively (reproduced from [94]; Copyright 2022, American Chemical Society).

4. Critical Challenges and Future Perspectives in Complex Environments

Despite the remarkable progress in developing high-performance MOF-derived VOC sensors in laboratory settings, several critical challenges must be overcome to enable their transition into practical, real-world applications. The ambient environment is not a clean, controlled system; it is a complex and dynamic mixture of multiple gases, fluctuating humidity, and temperature variations. Addressing the issues of selectivity, humidity interference, and long-term stability is paramount for the successful deployment of these promising sensor technologies. In practical indoor/outdoor settings, VOC sensors experience multi-analyte atmospheres alongside RH 10–95% and modest $\Delta T \approx 5$–15 °C. Humidity competes for adsorption sites, forms surface hydroxyls, and perturbs depletion layers, generating baseline shifts, slower recovery, and apparent sensitivity changes. Cross-sensitivity arises when common interferents (e.g., ethanol, isopropanol, methanol, acetone) react with pre-adsorbed oxygen or occupy catalytic sites, while oxidants (NO_2/O_3) can invert or exaggerate responses through electron withdrawal. We therefore recommend reporting (i) response at $\geq$3 RH levels (e.g., 20/50/80%), (ii) cross-response matrices for typical indoor interferents (alcohols/ketones/aromatics) and NO_2, and (iii) temperature-ramp robustness. Anti-humidity strategies include hydrophobic overlayers (e.g., PDMS or fluoropolymer skins) that repel water yet pass VOCs, often stabilizing responses up to ~90% RH; defect/interface engineering in MOF-derived oxides (oxygen-vacancy enrichment, p–n junctions) that lowers activation barriers and improves signal-to-noise at $\leq$250 °C; and

array-level analytics (LDA/k-NN/NN) that resolve mixtures/isomers even when each channel is cross-sensitive.

4.1. The Selectivity and Anti-Interference Conundrum

Perhaps the most significant hurdle for any chemical sensor is selectivity: the ability to detect a specific target analyte without being misled by the presence of other, often more abundant, interfering compounds [104]. This challenge has given rise to two distinct, and at times competing, philosophical approaches: building selectivity into the material itself (intrinsic selectivity) or designing a system that can learn to distinguish patterns (extrinsic selectivity).

The intrinsic approach aims to engineer a sensing material with a uniquely strong affinity or high catalytic activity for a single target molecule. In the context of MOF-derived materials, this can be pursued by tuning the pore size of the precursor MOF to create a molecular sieving effect [105], where only molecules below a certain kinetic diameter can access the active sites. Another strategy involves the post-synthetic modification or functionalization of the MOF precursor with chemical groups that have a specific affinity for the target analyte, a property that may be partially retained in the derivative [106]. While elegant, achieving true intrinsic selectivity is exceptionally difficult, especially for discriminating between VOCs with similar sizes and chemical functionalities (e.g., ethanol vs. methanol).

The extrinsic approach, conversely, embraces the cross-sensitive nature of most sensor materials. In this paradigm, often called an "electronic nose" (e-nose), an array of several different sensors, each with a slightly different but overlapping response profile, is exposed to the gas mixture. While no single sensor is perfectly selective, the combined response pattern of the entire array acts as a unique "fingerprint" for a given analyte or mixture. MOF-derived materials are exceptionally well-suited for this approach, as the vast tunability of MOF precursors allows for the creation of a diverse library of sensing materials with varied selectivities [107]. The key to unlocking the potential of this approach lies in data processing. Machine learning (ML) algorithms, such as linear discriminant analysis (LDA), k-nearest neighbors (k-NN), and neural networks, are employed to analyze the high-dimensional data from the sensor array [108]. These algorithms can be trained to recognize the specific response patterns associated with different VOCs and their mixtures, achieving high classification accuracies (often > 95%) even in complex backgrounds [109–111]. The debate in the field centers on the robustness of these two approaches: while intrinsic selectivity is more universal, it is difficult to achieve; extrinsic selectivity is highly effective but may be less reliable when exposed to novel interferents not included in the training data. The most practical path forward likely involves a hybrid strategy, using an array of materials with enhanced, albeit imperfect, intrinsic selectivity to generate more easily distinguishable patterns for ML analysis. Table 4 provides a critical comparison of these strategies.

Two recent case studies help quantify the trade-offs. First, an intrinsic strategy using a Sn-MOF precursor to engineer laminar SnO_2 with abundant adsorbed oxygen delivered a response of ~10,000 toward 10 ppm formaldehyde at just 120 °C, with a sub-10 ppb detection limit and ~33/142 s response/recovery. The authors attribute the selectivity window to vacancy-rich surfaces and the nanoparticle-piled porous architecture that accelerates HCHO oxidation while suppressing cross-responses, illustrating how defect chemistry and microstructure control can approximate "intrinsic" selectivity in practice [112]. Second, embracing extrinsic selectivity, a six-channel MOF-film e-nose (HKUST-1, Cu(BDC), Cu(BPDC), UiO-66/67/68-NH_2 on QCMs) used k-nearest neighbors to discriminate 16 pure/mixture classes of xylene isomers with 96.5% accuracy at 100 ppm and 85.7% at 10 ppm; individual sensors showed limits of detection in the ~0.7–1.9 ppm range.

Importantly, the pore-geometry–driven sorption (Henry-region linearity up to ~100 ppm) underpinned the separability of feature vectors, making the array robust to isomeric similarity while still relying on pattern recognition [110]. Critically, these examples expose complementary vulnerabilities. The MOF-derived SnO_2 case achieves spectacular single-analyte figures at low temperature, but its performance hinges on finely tuned vacancy populations and surface oxygen speciation; selectivity may narrow outside aldehyde-like chemistries or under humidity excursions, demanding rigorous stability and cross-matrix testing before generalization [112]. By contrast, the MOF-film array demonstrates that pattern-based selectivity scales to mixtures and isomers—but accuracy falls as concentration drops (96.5% → 85.7%), reflecting reduced signal-to-noise and the well-known brittleness of models under domain shift (unseen interferents, humidity drift) [110]. A pragmatic way forward is therefore a hybrid: use MOF-derived oxides to embed partial intrinsic filters (size/chemistry gating, catalytic bias) so that array responses become more linearly separable, then train ML with drift-aware protocols (temperature/humidity compensation, transfer learning and continual calibration). In this framing, "intrinsic" design enhances feature quality, while "extrinsic" analytics extracts robust decision boundaries—mitigating overfitting to curated interferent sets and preserving low-temperature operability in realistic, fluctuating backgrounds.

Table 4. Analysis of strategies for enhancing selectivity in complex VOC mixtures.

Strategy	Mechanism	Key Advantages	Major Limitations/Challenges	Representative Examples/Refs.
Intrinsic Selectivity				
Pore Engineering/Molecular Sieving	MOF precursor pores are sized to physically exclude larger interferents while allowing smaller target molecules to access active sites.	True physical selectivity based on size; can be highly effective for disparate molecules.	Difficult to discriminate between molecules of similar size; pore structure may change during pyrolysis.	[69]
Surface Functionalization/Doping	Active sites are chemically modified to have a specific affinity (e.g., Lewis acid/base interaction) for the target VOC.	Can provide selectivity based on chemical properties, not just size. Doping can enhance catalytic activity for a specific reaction.	Functional groups may not survive pyrolysis; achieving high specificity is challenging.	[106]
Extrinsic Selectivity				
Sensor Array + Machine Learning	An array of cross-sensitive sensors generates a unique response pattern ("fingerprint") for each analyte, which is classified by an ML algorithm.	Highly effective for discriminating components in known mixtures (>95% accuracy); pragmatic approach.	Requires a training dataset; performance may degrade with novel, untrained interferents; adds system complexity.	[113]

4.2. Mitigating Humidity-Induced Performance Degradation

Water vapor is the most pervasive and problematic interferent in real-world sensing applications [114]. Water molecules can competitively adsorb onto the active sites of the sensor, blocking them from the target VOC. They can also directly participate in surface reactions, altering the baseline resistance of the sensor and leading to significant signal drift and inaccurate readings [115]. Furthermore, many MOF structures themselves

are susceptible to hydrolysis, which can cause irreversible degradation of the material. Overcoming this humidity challenge is a prerequisite for any practical VOC sensor.

Similar to the selectivity challenge, strategies to impart humidity tolerance can be categorized as intrinsic or extrinsic. The intrinsic approach focuses on designing the sensing material to be inherently hydrophobic. This can be achieved by synthesizing the precursor MOF with non-polar, water-repelling organic linkers, which can impart a hydrophobic character to the final derived material [116]. For example, incorporating methyl or other alkyl groups onto the linker can effectively shield the metal-oxygen bonds from attack by water molecules.

The extrinsic approach involves physically isolating the hydrophilic sensing material from ambient moisture by applying a protective barrier. A highly successful strategy is to coat the sensor with a thin, gas-permeable, but hydrophobic polymer layer, such as polydimethylsiloxane (PDMS) [117]. The PDMS film acts as a semi-permeable membrane, effectively repelling polar water molecules while allowing non-polar or less polar VOC molecules to diffuse through and reach the sensing layer. This method has been shown to dramatically improve sensor stability and performance in high-humidity environments (up to 90% RH). Figure 7 illustrates the concept of a hydrophobic MOF/polymer composite sensor. Other strategies include operating the sensor at elevated temperatures to promote water desorption or using UV light to provide the energy needed to remove adsorbed water molecules at room temperature [118]. Each approach presents a trade-off: intrinsic hydrophobicity can be difficult to achieve without compromising other properties, while extrinsic coatings may slightly increase the sensor's response time or block larger VOC molecules. A critical evaluation of these methods is presented in Table 5.

Table 5. Critical evaluation of methods for mitigating humidity interference.

Mitigation Strategy	Working Principle	Effectiveness (RH Range)	Pros	Cons	Key References
Hydrophobic MOF Linkers	Intrinsic hydrophobicity of the material repels water molecules from active sites.	Varies; can be effective up to moderate RH.	No additional layers; does not impede gas diffusion.	Difficult to synthesize stable, highly porous hydrophobic MOFs; may reduce affinity for polar VOCs.	[116]
Hydrophobic Polymer Coating (e.g., PDMS)	A gas-permeable, water-repellent physical barrier is coated on the sensor.	Highly effective, up to 90–100% RH.	Can be applied to a wide range of sensing materials; excellent water resistance.	May increase response/recovery time; potential for pore blocking or swelling; may reduce sensitivity to large VOCs.	[117]
UV-Assisted Desorption	UV light provides energy to desorb water molecules from the sensor surface at RT.	Effective for improving RT performance under humidity.	Enables low-power, RT operation.	Requires an external UV source, increasing system complexity and power consumption.	[7]
Algorithmic Compensation	A separate humidity sensor is used, and an algorithm corrects the VOC sensor's output based on the measured RH.	Can be effective if the relationship between humidity and response is well-characterized.	Can be implemented in software; does not modify the sensor material.	Requires dual sensors; complex calibration; may fail under rapid humidity changes.	[113]

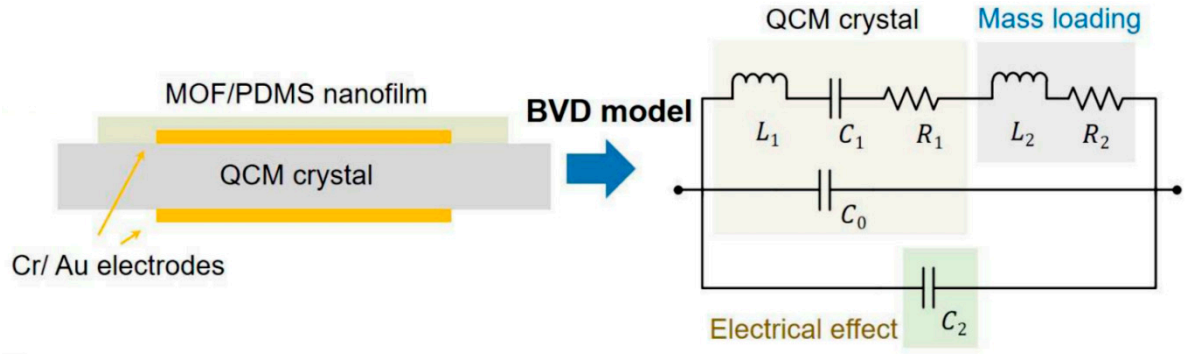


Figure 7. Schematic of a hydrophobic composite sensor for humidity-resistant VOC detection. A hydrophilic MOF sensing layer is coated with a hydrophobic polymer (e.g., PDMS), which blocks water molecules while allowing target VOCs to permeate (reproduced from [118]; Copyright 2024, American Chemical Society).

4.3. Bridging the Gap to Application: Stability, Reproducibility, and Scalability

Beyond performance in complex environments, several engineering and manufacturing hurdles represent a significant barrier to the commercialization of MOF-derived sensors. First, long-term stability and sensor drift are major concerns. The nanostructured materials can undergo gradual changes over time due to thermal stress, chemical attack, or irreversible adsorption of contaminants, leading to a decline in performance and requiring frequent recalibration [119]. Second, batch-to-batch reproducibility remains a formidable challenge. The solvothermal synthesis methods commonly used to produce MOFs are sensitive to minor variations in temperature, pressure, and reactant concentrations, which can lead to significant differences in the properties of materials produced in different batches [113]. This lack of consistency is a critical failure point for mass production, where every sensor must perform within tight specifications. Finally, the scalability of synthesis is a largely unaddressed issue in the academic literature [120]. Most reported syntheses are performed at the milligram or gram scale, whereas commercial applications would require production at the kilogram scale or beyond. Traditional batch-based solvothermal methods are ill-suited for large-scale production due to long reaction times and safety concerns [121]. Overcoming this "scalability gap" will require a shift in research focus towards developing robust, continuous-flow synthesis methods that can produce high-quality materials reliably and cost-effectively [122]. Without dedicated efforts to solve these fundamental manufacturing challenges, even the most sensitive and selective lab-scale sensor will remain an academic curiosity.

4.4. Future Outlook and Emerging Frontiers

The field of MOF-derived sensors is dynamic and rapidly evolving, with several exciting frontiers poised to address the current limitations and unlock new capabilities.

Novel Device Architectures: The integration of MOF-derived materials into novel device platforms is a key area of development. There is growing interest in fabricating flexible, stretchable, and wearable chemiresistive sensors for applications in personalized health monitoring (e.g., skin-worn patches for detecting VOCs in sweat) and soft robotics. This requires developing new methods to deposit and pattern MOF-derived films onto flexible substrates while maintaining their structural integrity and performance under mechanical strain.

Emerging Composite Materials: The exploration of new hybrid materials that combine MOF-derivatives with other advanced nanomaterials offers a promising route to synergistic performance enhancements [123]. For example, composites of MOF-derived oxides with 2D materials like MXenes or graphene can offer superior conductivity and unique

surface chemistry [124]. MOF-polymer composites are also being investigated to improve mechanical stability and processability while also providing an additional mechanism for tuning selectivity [125].

Computational Co-Design: The sheer combinatorial space of possible MOF precursors is too vast to explore experimentally. High-throughput computational screening, guided by machine learning, is emerging as an indispensable tool to accelerate the discovery of new materials [126]. By training ML models on large databases of calculated or experimental MOF properties, researchers can rapidly predict the most promising precursor structures for yielding derivatives with optimal catalytic activity or adsorption properties for a specific VOC, dramatically streamlining the materials discovery pipeline [127]. Figure 8 illustrates the concept of ML-assisted materials screening.

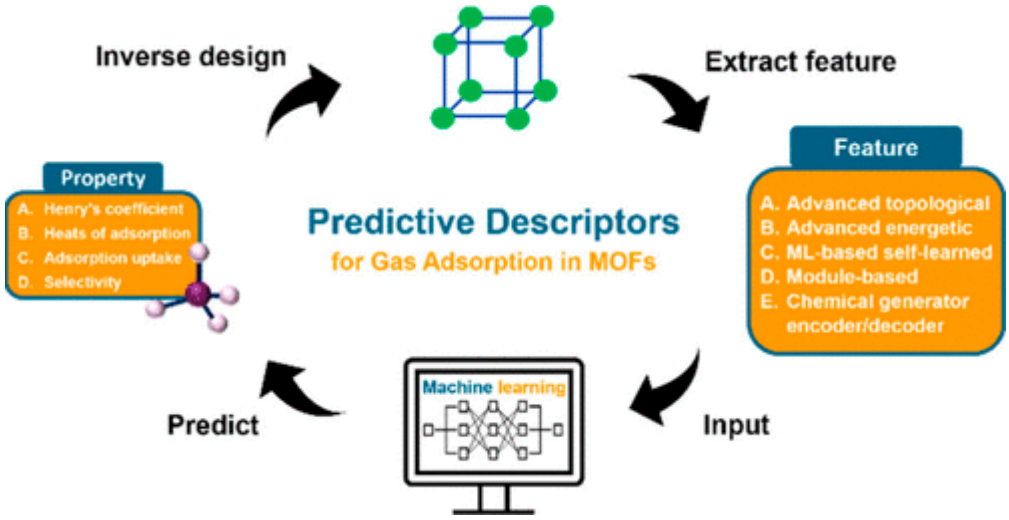


Figure 8. Workflow for machine learning-assisted discovery of MOFs for gas adsorption applications. ML models are trained on features from known MOFs to predict the performance of hypothetical structures, accelerating the identification of top candidates (reproduced from [126]; Under a Creative Commons license, Copyright 2025, American Chemical Society).

Advanced Operando Characterization: To resolve lingering questions about sensing mechanisms, particularly the dynamic evolution of the catalyst surface during operation, there is a critical need for more advanced operando characterization techniques. While in-situ DRIFTS provides chemical information, techniques like operando X-ray Photoelectron Spectroscopy (XPS) and X-ray Absorption Spectroscopy (XAS) can provide real-time information about the oxidation state and local coordination environment of the metal centers during the chemiresistive sensing process [128]. Such studies will be invaluable for building a complete, dynamic picture of the catalytic interface at work and for definitively linking material structure to function.

In conclusion, MOF-derived catalytic interfaces represent a highly promising and rapidly advancing frontier in the development of low-temperature chemiresistive VOC sensors. By leveraging MOFs as sacrificial templates, researchers have created a new generation of materials with tailored porosity, engineered heterojunctions, and abundant catalytic active sites, leading to unprecedented sensitivity and low-temperature performance. While significant challenges related to selectivity, humidity tolerance, and manufacturability remain, the ongoing innovation in material synthesis, device integration, computational design, and advanced characterization provides a clear and exciting path toward the realization of practical, high-performance sensors for a healthier and safer environment.

Author Contributions: Conceptualization, L.F. and S.Z.; methodology, L.F. and S.Z.; software, L.Z. and J.Z.; validation, L.Z. and J.Z.; formal analysis, L.Z. and J.Z.; writing—original draft preparation, L.Z., S.Z. and J.Z.; writing—review and editing, L.F.; supervision, L.F. and S.Z.; project administration, L.F. All authors have read and agreed to the published version of the manuscript.

Funding: This research received no external funding.

Data Availability Statement: Data sharing not applicable.

Conflicts of Interest: The authors declare no conflicts of interest.

References

1. Epping, R.; Koch, M. On-Site Detection of Volatile Organic Compounds (VOCs). *Molecules* **2023**, *28*, 1598. [CrossRef] [PubMed]
2. Meng, X.; Wang, Y.; Song, X.; Liu, Y.; Xie, Y.; Xu, L.; Yu, J.; Qiu, L.; Wang, X.; Lin, J. Application and Development of SERS Technology in Detection of VOC Gases. *Mater. Chem. Front.* **2025**, *9*, 349–366. [CrossRef]
3. Meng, F.; Yuan, Z.; Meng, D. Chemical Sensors for Volatile Organic Compound Detection. *Chemosensors* **2023**, *11*, 553. [CrossRef]
4. Li, X.-B.; Yuan, B.; Huangfu, Y.; Yang, S.; Song, X.; Qi, J.; He, X.; Wang, S.; Chen, Y.; Yang, Q.; et al. Vertical Changes in Volatile Organic Compounds (VOCs) and Impacts on Photochemical Ozone Formation. *Atmos. Chem. Phys.* **2025**, *25*, 2459–2472. [CrossRef]
5. Pathak, A.K.; Swargiary, K.; Kongsawang, N.; Jitpratak, P.; Ajchareeyasoontorn, N.; Udomkittivorakul, J.; Viphavakit, C. Recent Advances in Sensing Materials Targeting Clinical Volatile Organic Compound (VOC) Biomarkers: A Review. *Biosensors* **2023**, *13*, 114. [CrossRef]
6. Chen, X.; Behboodian, R.; Bagnall, D.; Taheri, M.; Nasiri, N. Metal-Organic-Frameworks: Low Temperature Gas Sensing and Air Quality Monitoring. *Chemosensors* **2021**, *9*, 316. [CrossRef]
7. Wang, Y.; Zhou, X.; Mao, S.; Chen, S.; Guo, Z. Challenges and Applications of Bio-Sniffers for Monitoring Volatile Organic Compounds in Medical Diagnostics. *Chemosensors* **2025**, *13*, 127. [CrossRef]
8. Zhang, C.; Qian, L.; Zeng, W. MOS Based Gas Sensor in Detection of Volatile Organic Compounds: A Review. *Sens. Actuators Phys.* **2025**, *393*, 116818. [CrossRef]
9. Kim, T.; Kim, Y.; Cho, W.; Kwak, J.-H.; Cho, J.; Pyeon, Y.; Kim, J.J.; Shin, H. Ultralow-Power Single-Sensor-Based E-Nose System Powered by Duty Cycling and Deep Learning for Real-Time Gas Identification. *ACS Sens.* **2024**, *9*, 3557–3572. [CrossRef]
10. Ochoa-Muñoz, Y.H.; Mejía de Gutiérrez, R.; Rodríguez-Páez, J.E. Metal Oxide Gas Sensors to Study Acetone Detection Considering Their Potential in the Diagnosis of Diabetes: A Review. *Molecules* **2023**, *28*, 1150. [CrossRef]
11. Khandelwal, G.; Deswal, S.; Dahiya, R. Triboelectric Nanogenerators as Power Sources for Chemical Sensors and Biosensors. *ACS Omega* **2022**, *7*, 44573–44590. [CrossRef]
12. So, S.H.; Lee, S.Y.; Kang, H.; Min, H.; Jung, H.-T.; Lee, K.H.; Kim, D. Metal-Organic Frameworks for Gas Sensors: Comprehensive Review from Principal, Fabrication to Application. *Int. J. Extrem. Manuf.* **2025**, *8*, 012001. [CrossRef]
13. Ma, T.; Ma, J.-G.; Cheng, P. Metal-Organic Frameworks as Electrochemical Sensors. In *Metal-Organic Frameworks in Analytical Sample Preparation and Sensing*; Elsevier: Amsterdam, The Netherlands, 2024; pp. 305–342.
14. Abid, H.R.; Azhar, M.R.; Iglauer, S.; Rada, Z.H.; Al-Yaseri, A.; Keshavarz, A. Physicochemical Characterization of Metal Organic Framework Materials: A Mini Review. *Heliyon* **2024**, *10*, e23840. [CrossRef]
15. Rasheed, T.; Anwar, M.T. Metal Organic Frameworks as Self-Sacrificing Modalities for Potential Environmental Catalysis and Energy Applications: Challenges and Perspectives. *Coord. Chem. Rev.* **2023**, *480*, 215011. [CrossRef]
16. Huang, B.; Li, Y.; Zeng, W. Application of Metal-Organic Framework-Based Composites for Gas Sensing and Effects of Synthesis Strategies on Gas-Sensitive Performance. *Chemosensors* **2021**, *9*, 226. [CrossRef]
17. Wei, H.; Zhang, H.; Song, B.; Yuan, K.; Xiao, H.; Cao, Y.; Cao, Q. Metal–Organic Framework (MOF) Derivatives as Promising Chemiresistive Gas Sensing Materials: A Review. *Int. J. Environ. Res. Public Health* **2023**, *20*, 4388. [CrossRef] [PubMed]
18. Chen, L.-N.; Li, H.-Q.; Yan, M.-W.; Yuan, C.-F.; Zhan, W.-W.; Jiang, Y.-Q.; Xie, Z.-X.; Kuang, Q.; Zheng, L.-S. Ternary Alloys Encapsulated within Different MOFs via a Self-Sacrificing Template Process: A Potential Platform for the Investigation of Size-Selective Catalytic Performances. *Small* **2017**, *13*, 1700683. [CrossRef] [PubMed]
19. Yuan, H.; Li, N.; Fan, W.; Cai, H.; Zhao, D. Metal-Organic Framework Based Gas Sensors. *Adv. Sci.* **2022**, *9*, 2104374. [CrossRef]
20. Majhi, S.M.; Ali, A.; Rai, P.; Greish, Y.E.; Alzamly, A.; Surya, S.G.; Qamhieh, N.; Mahmoud, S.T. Metal–Organic Frameworks for Advanced Transducer Based Gas Sensors: Review and Perspectives. *Nanoscale Adv.* **2022**, *4*, 697–732. [CrossRef]
21. Feng, H.; Guo, S.; Guo, Y.; Zhao, Q.; Xia, Y.; Duan, Z.; Hou, M.; Yang, L.; Gao, L.; Tai, H. Advances in Metal-Organic Framework-Based Hydrogen Sulfide Gas Sensors. *Coord. Chem. Rev.* **2026**, *546*, 217087. [CrossRef]

22. Huang, Y.; Chen, Y.; Xu, M.; Ly, A.; Gili, A.; Murphy, E.; Asset, T.; Liu, Y.; De Andrade, V.; Segre, C.U.; et al. Catalysts by Pyrolysis: Transforming Metal-Organic Frameworks (MOFs) Precursors into Metal-Nitrogen-Carbon (MNC) Materials. *Mater. Today* **2023**, *69*, 66–78. [CrossRef]
23. Wang, X.-F.; Song, X.-Z.; Sun, K.-M.; Cheng, L.; Ma, W. MOFs-Derived Porous Nanomaterials for Gas Sensing. *Polyhedron* **2018**, *152*, 155–163. [CrossRef]
24. Zhang, J.; Wang, J.; Long, S.; Peh, S.B.; Dong, J.; Wang, Y.; Karmakar, A.; Yuan, Y.D.; Cheng, Y.; Zhao, D. Luminescent Metal–Organic Frameworks for the Detection and Discrimination of o-Xylene from Xylene Isomers. *Inorg. Chem.* **2018**, *57*, 13631–13639. [CrossRef]
25. Chen, Y.-Z.; Zhang, R.; Jiao, L.; Jiang, H.-L. Metal–Organic Framework-Derived Porous Materials for Catalysis. *Coord. Chem. Rev.* **2018**, *362*, 1–23. [CrossRef]
26. Chen, K.; Bai, S.; Li, H.; Xue, Y.; Zhang, X.; Liu, M.; Jia, J. The Co_3O_4 Catalyst Derived from ZIF-67 and Their Catalytic Performance of Toluene. *Appl. Catal. Gen.* **2020**, *599*, 117614. [CrossRef]
27. Zhang, X.; Xiang, S.; Du, Q.; Bi, F.; Xie, K.; Wang, L. Effect of Calcination Temperature on the Structure and Performance of Rod-like MnCeOx Derived from MOFs Catalysts. *Mol. Catal.* **2022**, *522*, 112226. [CrossRef]
28. da Silva Gropelo, H.; dos Santos Theodoro, R.; dos Santos, G.S.M.; Perfecto, T.M.; Volanti, D.P. Crystallite Size Control in MOF-5-Derived Nanostructured ZnO Sensors for Detecting 1-Pentanol. *J. Alloys Compd.* **2025**, *1036*, 181745. [CrossRef]
29. Shen, B.; Yuan, T.; Zhang, W.; Chen, Y.; Xu, J. Complex Shell Fe-ZnO Derived from ZIF-8 as High-Quality Acetone MEMS Sensor. *Chin. Chem. Lett.* **2024**, *35*, 109490. [CrossRef]
30. Xian, J.; Li, J.; Wang, W.; Zhu, J.; Li, P.; Leung, C.M.; Zeng, M.; Lu, X.; Gao, X.; Liu, J.-M. Enhanced Specific Surface Area of ZIF-8 Derived ZnO Induced by Sulfuric Acid Modification for High-Performance Acetone Gas Sensor. *Appl. Surf. Sci.* **2023**, *614*, 156175. [CrossRef]
31. Guo, R.; Hou, X.; Shi, C.; Zhang, W.; Zhou, Y. MOF-Derived Co_3O_4 Hierarchical Porous Structure for Enhanced Acetone Sensing Performance with High Sensitivity and Low Detection Limit. *Sens. Actuators B Chem.* **2023**, *376*, 132973. [CrossRef]
32. Li, C.; Zhou, N.; Xia, Z.; Yan, C. UiO-66 for Composite Template Derived Cu/Zr-O with Dodecahedral Structure for Efficient Asymmetry Supercapacitor. *J. Power Sources* **2024**, *623*, 235506. [CrossRef]
33. Hua, M.; Wang, S.; Cheng, M.; Liang, G.; Xu, L.; Zhou, Y. The Application of TiO2@ UiO-66-(OH) 2 Composites for the Photocatalytic Degradation of Gaseous Formaldehyde under Visible Light. *J. Photochem. Photobiol. Chem.* **2025**, *464*, 116328. [CrossRef]
34. Guo, W.; Niu, J.; Hong, B.; Xu, J.; Han, Y.; Peng, X.; Ge, H.; Li, J.; Zeng, Y.; Wang, X. Mesoporous Co_3O_4/In_2O_3 Nanocomposites for Formaldehyde Gas Sensors: Synthesis from ZIF-67 and Gas-Sensing Behavior. *Mater. Res. Bull.* **2023**, *164*, 112264. [CrossRef]
35. Pérez-Mayoral, E.; Godino-Ojer, M.; Matos, I.; Bernardo, M. Opportunities from Metal Organic Frameworks to Develop Porous Carbons Catalysts Involved in Fine Chemical Synthesis. *Catalysts* **2023**, *13*, 541. [CrossRef]
36. Zhang, X.; Lan, W.; Xu, J.; Luo, Y.; Pan, J.; Liao, C.; Yang, L.; Tan, W.; Huang, X. ZIF-8 Derived Hierarchical Hollow ZnO Nanocages with Quantum Dots for Sensitive Ethanol Gas Detection. *Sens. Actuators B Chem.* **2019**, *289*, 144–152. [CrossRef]
37. Liu, L.; Wang, Y.; Guan, K.; Liu, Y.; Li, Y.; Sun, F.; Wang, X.; Zhang, C.; Feng, S.; Zhang, T. Influence of Oxygen Vacancies on the Performance of SnO_2 Gas Sensing by Near-Ambient Pressure XPS Studies. *Sens. Actuators B Chem.* **2023**, *393*, 134252. [CrossRef]
38. Frankcombe, T.J.; Liu, Y. Interpretation of Oxygen 1s X-Ray Photoelectron Spectroscopy of ZnO. *Chem. Mater.* **2023**, *35*, 5468–5474. [CrossRef]
39. Gadipelli, S.; Guo, Z.X. Tuning of ZIF-Derived Carbon with High Activity, Nitrogen Functionality, and Yield—A Case for Superior CO_2 Capture. *ChemSusChem* **2015**, *8*, 2123–2132. [CrossRef]
40. Jo, Y.-M.; Kim, T.-H.; Lee, C.-S.; Lim, K.; Na, C.W.; Abdel-Hady, F.; Wazzan, A.A.; Lee, J.-H. Metal–Organic Framework-Derived Hollow Hierarchical Co_3O_4 Nanocages with Tunable Size and Morphology: Ultrasensitive and Highly Selective Detection of Methylbenzenes. *ACS Appl. Mater. Interfaces* **2018**, *10*, 8860–8868. [CrossRef]
41. Jiang, S.; Li, W.; Liu, J.; Jiang, J.; Zhang, Z.; Shang, W.; Peng, N.; Wen, Y. ZnO@ZIF-8 Core-Shell Structure Nanorods Superhydrophobic Coating on Magnesium Alloy with Corrosion Resistance and Self-Cleaning. *J. Magnes. Alloys* **2023**, *11*, 3287–3301. [CrossRef]
42. Qin, W.; Zhang, Z.; Xu, X.; Xiao, Y.; Meng, F. Bimetallic Organic Framework-Derived Porous Co_3O_4/Fe_2O_3 Nanosheets for Acetone Sensing. *Sci. Rep.* **2025**, *15*, 20912. [CrossRef]
43. Wang, Y.; Huang, J.; Tang, W.; Long, M.; Zhang, Z.; Liu, H.; An, D. Highly Sensitive Triethylamine Sensor Based on MOF-Derived Bimetallic NiO-SnO_2 Nanomaterials. *Ceram. Int.* **2025**, *51*, 9329–9342. [CrossRef]
44. Li, X.-B.; Sun, S.; Hu, X.; Zhang, Q.-Q.; Gao, C.; Zhou, H.; Wu, B.-X.; Wang, A.-Q.; Hu, W.-Y.; Wang, Y.-J.; et al. Fabrication and Performance Enhancement of an $In_2O_3/BiVO_4$ Heterojunction for N-Butanol Gas Sensing Applications. *RSC Adv.* **2024**, *14*, 39715–39726. [CrossRef]
45. Fan, X.; Yang, S.; Huang, C.; Lu, Y.; Dai, P. Preparation and Enhanced Acetone-Sensing Properties of ZIF-8-Derived Co_3O_4@ ZnO Microspheres. *Chemosensors* **2023**, *11*, 376. [CrossRef]

46. Song, P.; Sun, F.; Luan, T.; Meng, Q.; Geng, W. MOF-Derived In_2O_3/$BiVO_4$ Composites for Sensitive and Trace Detection of n-C4H9OH. *ACS Sens.* **2025**, *10*, 5589–5599. [CrossRef]
47. Mohamed, R.M.; Shawky, A. Visible-Light-Driven Hydrogen Production over ZIF-8 Derived Co_3O_4/ZnO S-Scheme Based p-n Heterojunctions. *Opt. Mater.* **2022**, *124*, 112012. [CrossRef]
48. Wang, G.; Yang, S.; Cao, L.; Jin, P.; Zeng, X.; Zhang, X.; Wei, J. Engineering Mesoporous Semiconducting Metal Oxides from Metal-Organic Frameworks for Gas Sensing. *Coord. Chem. Rev.* **2021**, *445*, 214086. [CrossRef]
49. Xiong, Y.; Xu, W.; Zhu, Z.; Xue, Q.; Lu, W.; Ding, D.; Zhu, L. ZIF-Derived Porous ZnO-Co_3O_4 Hollow Polyhedrons Heterostructure with Highly Enhanced Ethanol Detection Performance. *Sens. Actuators B Chem.* **2017**, *253*, 523–532. [CrossRef]
50. Zayeri, S.; Asl, S.; Mehrasa, S.; Saboor, F.; Safajoo-Jahankhanemlou, M. Inhibition Semiconductor Gas Sensors Based on Hollow Metal Oxides: Focusing on MOF-Derived Structures. *Prog. Chem. Biochem. Res.* **2025**, *8*, 304–329.
51. Zhou, W.; Wu, Y.-P.; Zhao, J.; Dong, W.-W.; Qiao, X.-Q.; Hou, D.-F.; Bu, X.; Li, D.-S. Efficient Gas-Sensing for Formaldehyde with 3D Hierarchical Co_3O_4 Derived from Co_5-Based MOF Microcrystals. *Inorg. Chem.* **2017**, *56*, 14111–14117. [CrossRef]
52. Ma, X.; Zhou, X.; Gong, Y.; Han, N.; Liu, H.; Chen, Y. MOF-Derived Hierarchical ZnO/$ZnFe_2O_4$ Hollow Cubes for Enhanced Acetone Gas-Sensing Performance. *RSC Adv.* **2017**, *7*, 34609–34617. [CrossRef]
53. Duan, J.; He, X.; Fang, X.; Yue, J.; Chen, G.; Wang, W. The Composite of UiO-66 Derived ZrO2 and g-C3N4 for Oxidative Removal of Formaldehyde at the Room Temperature. *Diam. Relat. Mater.* **2022**, *129*, 109365. [CrossRef]
54. Liu, Z.; He, W.; Zhang, Q.; Shapour, H.; Bakhtari, M.F. Preparation of a GO/MIL-101(Fe) Composite for the Removal of Methyl Orange from Aqueous Solution. *ACS Omega* **2021**, *6*, 4597–4608. [CrossRef]
55. Cao, S.; Zhou, T.; Xu, X.; Bing, Y.; Sui, N.; Wang, J.; Li, J.; Zhang, T. Metal-Organic Frameworks Derived Inverse/Normal Bimetallic Spinel Oxides toward the Selective VOCs and H2S Sensing. *J. Hazard. Mater.* **2023**, *457*, 131734. [CrossRef]
56. Chen, B.; Wang, X.; Zhang, Q.; Xi, X.; Cai, J.; Qi, H.; Shi, S.; Wang, J.; Yuan, D.; Fang, M. Synthesis and Characterization of the Interpenetrated MOF-5. *J. Mater. Chem.* **2010**, *20*, 3758–3767. [CrossRef]
57. Liang, M.; Yan, Y.; Yang, J.; Liu, X.; Jia, R.; Ge, Y.; Li, Z.; Huang, L. In Situ-Derived N-Doped ZnO from ZIF-8 for Enhanced Ethanol Sensing in ZnO/MEMS Devices. *Molecules* **2024**, *29*, 1703. [CrossRef]
58. Sun, Y.; Fan, H.; Shang, Y.; Lei, L.; Zhu, S.; Wang, H.; Dong, W.; Al-Bahrani, M.; Wang, W.; Ma, L. MOF-5 Derived 3D ZnO/Ag Micro-Octahedra for Ultrahigh Response and Selective Triethylamine Detection at Low Temperature. *Sens. Actuators B Chem.* **2023**, *390*, 133975. [CrossRef]
59. Gao, X.; Hou, X.; Ma, Z.; Xiao, C.; Jia, L. Highly Dispersed Ag Nanocrystals Functionalized ZIF-8 Derived ZnO Hollow Structures for Superior Sensitive and Selective Detection of Nitric Oxide. *Sens. Actuators B Chem.* **2025**, *422*, 136646. [CrossRef]
60. Tan, J.; Hussain, S.; Ge, C.; Wang, M.; Shah, S.; Liu, G.; Qiao, G. ZIF-67 MOF-Derived Unique Double-Shelled Co_3O_4/$NiCo_2O_4$ Nanocages for Superior Gas-Sensing Performances. *Sens. Actuators B Chem.* **2020**, *303*, 127251. [CrossRef]
61. Xu, J.; Liu, S.; Liu, Y. Co_3O_4/ZnO Nanoheterostructure Derived from Core–Shell ZIF-8@ZIF-67 for Supercapacitors. *RSC Adv.* **2016**, *6*, 52137–52142. [CrossRef]
62. Xiao, D.; Wang, Y.; Zhang, D.; Liu, Y.; Wang, H.; Li, Y.; Wei, H.; Wang, S.; Sun, M.; Sun, M. CuO/ZnO Hollow Nanocages Derived from Metal−organic Frameworks for Ultra-High and Rapid Response H2S Gas Sensor. *Ceram. Int.* **2024**, *50*, 15767–15779. [CrossRef]
63. Chen, X.; Wang, X.; Liu, W.; Tian, H.; Du, Y.; Wei, H.; Tang, L. UiO-66 Derived ZrO2@C Catalysts for the Double-Bond Isomerization Reaction of 2-Butene. *RSC Adv.* **2023**, *13*, 15934–15941. [CrossRef]
64. Li, S.; Zhao, L.; Zhang, Y.; Wan, Y.; Wang, H.; Zhang, Q.; Tang, Y. A Robust ZrO2 Rectifier Layer Derived from UiO-66 Enable Ultra-High Nickel Cathodes with High Stability and Ion Transport Kinetics for Lithium-Ion Batteries. *J. Power Sources* **2024**, *608*, 234533. [CrossRef]
65. Huang, H.; Cheng, M.; Yin, J.; Zhang, J.; Kong, L.; Bu, X.-H. MIL-101(Fe)-Derived Iron Oxide/Carbon Anode for Lithium-Ion Batteries: Derivation Process Study and Performance Optimization. *Electrochim. Acta* **2022**, *426*, 140794. [CrossRef]
66. Chen, J.; Dong, J.; Yang, J.; Chen, Y. CoFe2O4 Nanocubes Derived by Prussian Blue Analogs for Detecting Dopamine. *Microchem. J.* **2024**, *199*, 109999. [CrossRef]
67. Khan, F.U.; Mehmood, S.; Liu, S.; Xu, W.; Shah, M.N.; Zhao, X.; Ma, J.; Yang, Y.; Pan, X. A P-n Heterojunction Based Pd/PdO@ZnO Organic Frameworks for High-Sensitivity Room-Temperature Formaldehyde Gas Sensor. *Front. Chem.* **2021**, *9*, 742488. [CrossRef]
68. Li, J.; He, X.-Y.; Wang, X.; Lv, Y.; Ma, J.-G.; Li, B.; Cheng, P. Metal−Organic Framework-Derived Cu NWs@ZrO2 as a Highly Selective Catalyst for Methanol Synthesis from CO_2 Hydrogenation. *Inorg. Chem.* **2025**, *64*, 8448–8454. [CrossRef]
69. Shen, Y.; Tissot, A.; Serre, C. Recent Progress on MOF-Based Optical Sensors for VOC Sensing. *Chem. Sci.* **2022**, *13*, 13978–14007. [CrossRef]
70. Saruhan, B.; Lontio Fomekong, R.; Nahirniak, S. Influences of Semiconductor Metal Oxide Properties on Gas Sensing Characteristics. *Front. Sens.* **2021**, *2*, 657931. [CrossRef]
71. Liu, F.; Chen, X.; Jie, W.; Liu, Y.; Li, C.; Song, G.; Gong, X.; Liu, Q.; Qiu, M.; Ding, S.; et al. MOF-Derived High Oxygen Vacancies CuO/CeO2 Catalysts for Low-Temperature CO Preferential Oxidation. *J. Colloid Interface Sci.* **2024**, *674*, 778–790. [CrossRef]

72. Sun, S.; Xie, D.; Zhang, F.; Guo, W.; Qu, F. MOF-Derived NiO/γ-Fe_2O_3 p–n Heterojunctions for Ethylene Glycol Sensing. *J. Mater. Chem. C* **2025**. [CrossRef]
73. Chu, N.; Wang, Z.; Gu, F. Oxygen Vacancies Enabled MOF-Derived Tb–SnO_2 Compound for a High-Response, Low Detection Limit, and Humidity-Tolerant Chemiresistive Gas Sensor of Formaldehyde. *ACS Appl. Electron. Mater.* **2025**, *7*, 3041–3054. [CrossRef]
74. Han, J.; Kong, D.; Zhou, W.; Gao, Y.; Gao, Y.; Liu, G.; Lu, G. Interface-Engineering in MOF-Derived In_2O_3 for Highly Sensitive and Dual-Functional Gas Sensor towards NO2 and Triethylamine. *Sens. Actuators B Chem.* **2023**, *395*, 134491. [CrossRef]
75. Jossou, E.; Malakkal, L.; Dzade, N.Y.; Claisse, A.; Szpunar, B.; Szpunar, J. DFT + U Study of the Adsorption and Dissociation of Water on Clean, Defective, and Oxygen-Covered U3Si2{001}, {110}, and {111} Surfaces. *J. Phys. Chem. C Nanomater. Interfaces* **2019**, *123*, 19453–19467. [CrossRef] [PubMed]
76. Hu, J.; Xiong, X.; Guan, W.; Chen, Y.; Long, H. Regulation of O-Vacancy and Heterojunction Structure in MOF-Derived Fe_2O_3-Co_3O_4 Enhancing Acetone Sensing Performance. *Sens. Actuators B Chem.* **2024**, *401*, 135082. [CrossRef]
77. Deng, Z.; Zhang, Y.; Xu, D.; Zi, B.; Zeng, J.; Lu, Q.; Xiong, K.; Zhang, J.; Zhao, J.; Liu, Q. Ultrasensitive Formaldehyde Sensor Based on SnO_2 with Rich Adsorbed Oxygen Derived from a Metal Organic Framework. *ACS Sens.* **2022**, *7*, 2577–2588. [CrossRef]
78. Guo, R.; Deng, Y.; Jia, Y.; Shi, C.; Zhang, W.; Zhou, Y.; Hou, X. Gallium Ions Induced In-Situ MOF-Derived Hierarchical Porous Co_3O_4 for Ultra-High Acetone Response. *Sens. Actuators B Chem.* **2024**, *399*, 134832. [CrossRef]
79. Jin, W.; Zhang, N.; Jia, M.; Wang, J.; Yang, S.; Liu, Y.; Chen, W. Dual Functionalized Co_3O_4 Porous Cages with Pd and Co-MOF for Acetone Gas Sensing under High Humidity. *Mater. Today Commun.* **2024**, *40*, 109582. [CrossRef]
80. Ali, A.; Greish, Y.E.; Alzard, R.H.; Siddig, L.A.; Alzamly, A.; Qamhieh, N.; Mahmoud, S.T. Bismuth-Based Metal–Organic Framework as a Chemiresistive Sensor for Acetone Gas Detection. *Nanomaterials* **2023**, *13*, 3041. [CrossRef]
81. Bulemo, P.M.; Cheong, J.Y. MOF-Derived SnO_2 Hollow Spheres for Acetone Gas Sensing. *J. Mater. Sci. Mater. Electron.* **2023**, *34*, 1060. [CrossRef]
82. Zhu, L.; Wang, J.; Liu, J.; Nasir, M.S.; Zhu, J.; Li, S.; Liang, J.; Yan, W. Smart Formaldehyde Detection Enabled by Metal Organic Framework-Derived Doped Electrospun Hollow Nanofibers. *Sens. Actuators B Chem.* **2021**, *326*, 128819. [CrossRef]
83. Zhao, Q.; Xiang, N.; Wen, S.; Huo, H.; Li, Q. ZIF-67 Derived Cu-Co Mixed Oxides for Efficient Catalytic Oxidation of Formaldehyde at Low-Temperature. *Catalysts* **2023**, *13*, 117. [CrossRef]
84. Zhu, X.; Zhang, X.; Chang, X.; Li, J.; Pan, L.; Jiang, Y.; Gao, W.; Gao, C.; Sun, S. Metal-Organic Framework-Derived Porous SnO_2 Nanosheets with Grain Sizes Comparable to Debye Length for Formaldehyde Detection with High Response and Low Detection Limit. *Sens. Actuators B Chem.* **2021**, *347*, 130599. [CrossRef]
85. Ling, W.; Zhu, D.; Pu, Y.; Li, H. The Ppb-Level Formaldehyde Detection with UV Excitation for Yolk-Shell MOF-Derived ZnO at Room Temperature. *Sens. Actuators B Chem.* **2022**, *355*, 131294. [CrossRef]
86. Zhu, L.; Wang, Z.; Wang, J.; Liu, J.; Zhang, J.; Yan, W. Pt-Embedded Metal–Organic Frameworks Deriving Pt/ZnO-In_2O_3 Electrospun Hollow Nanofibers for Enhanced Formaldehyde Gas Sensing. *Chemosensors* **2024**, *12*, 93. [CrossRef]
87. Zou, M.; Dong, M.; Zhao, T. Advances in Metal-Organic Frameworks MIL-101 (Cr). *Int. J. Mol. Sci.* **2022**, *23*, 9396. [CrossRef]
88. Nikhar, S.; Chakraborty, M. Assessing the Photodegradation Efficiency of Benzene, Toluene, and Xylene (BTX): A Comparative Investigation Using Activated Charcoal (AC), Zeolitic Imidazolate Framework-8 (ZIF-8), and Zirconium Metal–Organic Framework (Zr-MOF). *Water Sci. Technol.* **2024**, *90*, 3193–3209. [CrossRef]
89. Theka, T.J.; Thamaga, B.R.J.; Tshabalala, Z.P.; Motsoeneng, R.G.; Swart, H.C.; Motaung, D.E. Fabrication of Metal-Organic Frameworks Derived Co_3O_4 Loaded on TiO2: Influence of Fe Loading on the Co_3O_4/TiO2 Heterostructure for Low-Ppm Benzene Detection. *Appl. Surf. Sci.* **2024**, *644*, 158789. [CrossRef]
90. Wu, W.J.; Hong, B.; Xu, J.; Peng, X.; Li, J.; Chen, H.; Qiu, S.; Zhang, N.; Wang, X. Ag/Co_3O_4 Nanocomposites from ZIF-67 MOF for Enhanced Low-Temperature Toluene Gas Sensing. *Phys. E Low-Dimens. Syst. Nanostructures* **2025**, *167*, 116174. [CrossRef]
91. Kang, Y.; Zhang, L.; Wang, W.; Yu, F. Ethanol Sensing Properties and First Principles Study of Au Supported on Mesoporous ZnO Derived from Metal Organic Framework ZIF-8. *Sensors* **2021**, *21*, 4352. [CrossRef] [PubMed]
92. Zhang, T.; Tang, X.; Zhang, J.; Zhou, T.; Wang, H.; Wu, C.; Xia, X.; Xie, C.; Zeng, D. Metal–Organic Framework-Assisted Construction of TiO2/Co_3O_4 Highly Ordered Necklace-like Heterostructures for Enhanced Ethanol Vapor Sensing Performance. *Langmuir* **2018**, *34*, 14577–14585. [CrossRef]
93. Zhang, Q.; Wang, H.; Ning, P.; Song, Z.; Liu, X.; Duan, Y. In Situ DRIFTS Studies on CuO-Fe_2O_3 Catalysts for Low Temperature Selective Catalytic Oxidation of Ammonia to Nitrogen. *Appl. Surf. Sci.* **2017**, *419*, 733–743. [CrossRef]
94. Fan, J.; Ren, Q.; Mo, S.; Sun, Y.; Fu, M.; Wu, J.; Chen, L.; Chen, P.; Ye, D. Transient In-Situ DRIFTS Investigation of Catalytic Oxidation of Toluene over α-, γ-and β-MnO2. *ChemCatChem* **2020**, *12*, 1046–1054. [CrossRef]
95. Gu, H.; Yokoya, T.; Kang, L.; Marlow, S.; Su, X.; Gong, M.; Yan, J.; Ren, Y.; Wang, Z.; Guan, X.; et al. Oxygen Vacancy Formation as the Rate-Determining Step in the Mars-van Krevelen Mechanism. *ChemRxiv* **2024**. [CrossRef]

96. Huang, Q.; Zhao, P.; Wang, W.; Lv, L.; Zhang, W.; Pan, B. In Situ Fabrication of Highly Dispersed Co–Fe-Doped-δ-MnO2 Catalyst by a Facile Redox-Driving MOFs-Derived Method for Low-Temperature Oxidation of Toluene. *ACS Appl. Mater. Interfaces* **2022**, *14*, 53872–53883. [CrossRef] [PubMed]
97. Mirzaei, A.; Kim, J.-H.; Kim, H.W.; Kim, S.S. Resistive-Based Gas Sensors for Detection of Benzene, Toluene and Xylene (BTX) Gases: A Review. *J. Mater. Chem. C* **2018**, *6*, 4342–4370. [CrossRef]
98. Xie, Y.; Lyu, S.; Zhang, Y.; Cai, C. Adsorption and Degradation of Volatile Organic Compounds by Metal–Organic Frameworks (MOFs): A Review. *Materials* **2022**, *15*, 7727. [CrossRef]
99. Wu, J.; Li, Z.; Luo, A.; Xing, X. A DFT Study of Volatile Organic Compounds Detection on Pristine and Pt-Decorated SnS Monolayers. *Sensors* **2023**, *23*, 7319. [CrossRef]
100. Ftahi, W.; Nusaibah, A.-S.; Yang, Y.; Tang, Y.; Liu, Q.; Ni, Y. ReaxFF Molecular Dynamics Study of Acetone and Ethanol Adsorption on ZnO Nanowires for Enhanced Gas Sensor Applications. *Appl. Surf. Sci.* **2025**, *716*, 164654. [CrossRef]
101. Zhan, M.; Xu, M.; Lin, W.; He, H.; He, C. Graphene Oxide Research: Current Developments and Future Directions. *Nanomaterials* **2025**, *15*, 507. [CrossRef]
102. Chang, X.; Li, K.; Qiao, X.; Xiong, Y.; Xia, F.; Xue, Q. ZIF-8 Derived ZnO Polyhedrons Decorated with Biomass Derived Nitrogen-Doped Porous Carbon for Enhanced Acetone Sensing. *Sens. Actuators B Chem.* **2021**, *330*, 129366. [CrossRef]
103. Ma, R.; Lei, H.; Han, M.; Hao, J. Recent Progress with Bismuth Sulfide for Room-Temperature Gas Sensing. *Chemosensors* **2025**, *13*, 120. [CrossRef]
104. Matavž, A.; Verstreken, M.F.; Boullart, L.; Tietze, M.L.; Sugihara, M.; Heinke, L.; Ameloot, R. Kinetic Selectivity in Metal-Organic Framework Chemical Sensors. *Nat. Commun.* **2025**, *16*, 8347. [CrossRef] [PubMed]
105. Gonçalves, B.F.; Fernández, E.; Valverde, A.; Gaboardi, M.; Salazar, H.; Petrenko, V.; Porro, J.M.; Cavalcanti, L.P.; Urtiaga, K.; Esperança, J.M.; et al. Exploring the Compositional Space of a Metal–Organic Framework with Ionic Liquids to Develop Porous Ionic Conductors for Enhanced Signal and Selectivity in VOC Capacitive Sensors. *J. Mater. Chem. A* **2024**, *12*, 14595–14607. [CrossRef]
106. Thuy Nguyen, L.H.; Mirzaei, A.; Kim, J.-Y.; Bach Phan, T.; Dai Tran, L.; Wu, K.C.-W.; Woo Kim, H.; Sub Kim, S.; Hoang Doan, T.L. Advancements in MOF-Based Resistive Gas Sensors: Synthesis Methods and Applications for Toxic Gas Detection. *Nanoscale Horiz.* **2025**, *10*, 1025–1053. [CrossRef]
107. Okur, S.; Hashem, T.; Bogdanova, E.; Hodapp, P.; Heinke, L.; Bräse, S.; Wöll, C. Optimized Detection of Volatile Organic Compounds Utilizing Durable and Selective Arrays of Tailored UiO-66-X SURMOF Sensors. *ACS Sens.* **2024**, *9*, 622–630. [CrossRef]
108. Okur, S.; Zhang, Z.; Sarheed, M.; Nick, P.; Lemmer, U.; Heinke, L. Towards a MOF E-Nose: A SURMOF Sensor Array for Detection and Discrimination of Plant Oil Scents and Their Mixtures. *Sens. Actuators B Chem.* **2020**, *306*, 127502. [CrossRef]
109. Sun, H.; Tian, F.; Liang, Z.; Sun, T.; Yu, B.; Yang, S.X.; He, Q.; Zhang, L.; Liu, X. Sensor Array Optimization of Electronic Nose for Detection of Bacteria in Wound Infection. *IEEE Trans. Ind. Electron.* **2017**, *64*, 7350–7358. [CrossRef]
110. Qin, P.; Day, B.A.; Okur, S.; Li, C.; Chandresh, A.; Wilmer, C.E.; Heinke, L. VOC Mixture Sensing with a MOF Film Sensor Array: Detection and Discrimination of Xylene Isomers and Their Ternary Blends. *ACS Sens.* **2022**, *7*, 1666–1675. [CrossRef] [PubMed]
111. Han, J.; Li, H.; Cheng, J.; Ma, X.; Fu, Y. Advances in Metal Oxide Semiconductor Gas Sensor Arrays Based on Machine Learning Algorithms. *J. Mater. Chem. C* **2025**, *13*, 4285–4303. [CrossRef]
112. Zong, S.; Zhang, Y.; Qin, C.; Bala, H.; Cao, J.; Wang, Y. Lanthanum Doped SnO/SnO_2 Rod-like Structure Sensors with High Sensitivity and Selectivity toward HCHO Detection. *J. Alloys Compd.* **2025**, *1010*, 177829. [CrossRef]
113. Benedetto, G.; Damacet, P.; Shehayeb, E.O.; Fabusola, G.; Simon, C.M.; Mirica, K.A. Metal–Organic Framework-Based Chemiresistive Array Paired with Machine Learning Algorithms for the Detection and Differentiation of Toxic Gases. *ACS Sens.* **2025**, *10*, 7787–7798. [CrossRef] [PubMed]
114. Gan, Z.; Zhou, Q.; Zheng, C.; Wang, J. Challenges and Applications of Volatile Organic Compounds Monitoring Technology in Plant Disease Diagnosis. *Biosens. Bioelectron.* **2023**, *237*, 115540. [CrossRef]
115. Wang, Y.; Zhou, Y. Recent Progress on Anti-Humidity Strategies of Chemiresistive Gas Sensors. *Materials* **2022**, *15*, 8728. [CrossRef]
116. Jasuja, H.; Huang, Y.; Walton, K.S. Adjusting the Stability of Metal–Organic Frameworks under Humid Conditions by Ligand Functionalization. *Langmuir* **2012**, *28*, 16874–16880. [CrossRef]
117. Cao, Y.; Fu, M.; Fan, S.; Gao, C.; Ma, Z.; Hou, D. Hydrophobic MOF/PDMS-Based QCM Sensors for VOCs Identification and Quantitative Detection in High-Humidity Environments. *ACS Appl. Mater. Interfaces* **2024**, *16*, 7721–7731. [CrossRef]
118. Singh, A.; Jhao, W.-C.; Chaudhary, P.; Lin, M.-F. UV-Enhanced, Humidity-Tolerant Formaldehyde Chemiresistor Based on Ce-MOF-Derived CeO2 Nanospheres Decorated 1D/2D Polyaniline Nanohybrid. *Adv. Mater. Technol.* **2025**, e01495. [CrossRef]
119. Zhang, R.; Lu, L.; Chang, Y.; Liu, M. Gas Sensing Based on Metal-Organic Frameworks: Concepts, Functions, and Developments. *J. Hazard. Mater.* **2022**, *429*, 128321. [CrossRef] [PubMed]
120. Xuan, Z. Machine-Learning-Assisted High-Throughput Screening of High-Performance MOFs for Multicomponent Gas Separation. *Ind. Eng. Chem. Res.* **2025**, *64*, 2926–2936. [CrossRef]

121. Lalawmpuia, R.; Lalhruaitluangi, M.; Lalhmunsiama; Tiwari, D. Metal Organic Framework (MOF): Synthesis and Fabrication for the Application of Electrochemical Sensing. *Environ. Eng. Res.* **2024**, *29*, 230636. [CrossRef]
122. Rubio-Martinez, M.; Hadley, T.D.; Batten, M.P.; Constanti-Carey, K.; Barton, T.; Marley, D.; Mönch, A.; Lim, K.-S.; Hill, M.R. Scalability of Continuous Flow Production of Metal–Organic Frameworks. *ChemSusChem* **2016**, *9*, 938–941. [CrossRef]
123. Zhuang, X.; Zhang, S.; Tang, Y.; Yu, F.; Li, Z.; Pang, H. Recent Progress of MOF/MXene-Based Composites: Synthesis, Functionality and Application. *Coord. Chem. Rev.* **2023**, *490*, 215208. [CrossRef]
124. Baba, T.; Janairo, L.G.; Maging, N.; Tañedo, H.S.; Concepcion, R.; Magdaong, J.J.; Bantang, J.P.; Del-amen, J.; Culaba, A. Advancements in Chemiresistive and Electrochemical Sensing Materials for Detecting Volatile Organic Compounds in Potato and Tomato Plants. *AgriEngineering* **2025**, *7*, 166. [CrossRef]
125. Tomić, M.; Šetka, M.; Vojk\uuvka, L.; Vallejos, S. VOCs Sensing by Metal Oxides, Conductive Polymers, and Carbon-Based Materials. *Nanomaterials* **2021**, *11*, 552. [CrossRef] [PubMed]
126. Sung, I.-T.; Cheng, Y.-H.; Hsieh, C.-M.; Lin, L.-C. Machine Learning for Gas Adsorption in Metal–Organic Frameworks: A Review on Predictive Descriptors. *Ind. Eng. Chem. Res.* **2025**, *64*, 1859–1875. [CrossRef]
127. Deeraj, B.; Jayan, J.S.; Raman, A.; Asok, A.; Paul, R.; Saritha, A.; Joseph, K. A Comprehensive Review of Recent Developments in Metal-Organic Framework/Polymer Composites and Their Applications. *Surf. Interfaces* **2023**, *43*, 103574. [CrossRef]
128. Fan, Y.; Wang, X.; Bo, G.; Xu, X.; See, K.W.; Johannessen, B.; Pang, W.K. Operando Synchrotron X-Ray Absorption Spectroscopy: A Key Tool for Cathode Material Studies in Next-Generation Batteries. *Adv. Sci.* **2025**, *12*, 2414480. [CrossRef] [PubMed]

Disclaimer/Publisher's Note: The statements, opinions and data contained in all publications are solely those of the individual author(s) and contributor(s) and not of MDPI and/or the editor(s). MDPI and/or the editor(s) disclaim responsibility for any injury to people or property resulting from any ideas, methods, instructions or products referred to in the content.